Calibrating the Simple Biosphere Model for Amazonian Tropical Forest Using Field and Remote Sensing Data. Part I: Average Calibration with Field Data

PIERS J. SELLERS, W. JAMES SHUTTLEWORTH†, AND JEFF L. DORMAN

Center for Ocean–Land–Atmosphere Research, Department of Meteorology, University of Maryland, College Park, Maryland

AMNON DALCHER

Sigma Data Computing Corporation, Rockville, Maryland

JOHN M. ROBERTS

Institute of Hydrology, Wallingford, Oxon, U.K.

(Manuscript received 30 April 1988, in final form 1 December 1988)

ABSTRACT

This paper describes the operation and calibration of the simple biosphere model (SiB) of Sellers et al. using micrometeorological and hydrological measurements taken in and above tropical forest in the central Amazon basin. The paper provides:

(i) an overview of the philosophy, structure and assumptions used in the model with particular reference to the tropical forest;
(ii) a review of the experimental systems and procedures used to obtain the field data; and
(iii) a specification of the physiological parameterization required in the model to provide an adequate average description of the data.

In the course of this study, it was found that some of the existing literature on stomatal behavior for tropical species is inconsistent with the observed behavior of the complete canopy in Amazonia and that the rainfall interception store of the canopy is considerably smaller than originally specified in SiB. Also the turbulent transfer model used in SiB was modified to account for the effects of height-varying foliage density. Finally, it was demonstrated that there is a distinct annual cycle in the biophysical properties of the forest canopy which influences the partitioning of energy into sensible and latent heat fluxes.

1. Introduction and model philosophy

In recent years, numerical experiments with general circulation models (GCMs) have demonstrated that the atmospheric circulation and rainfall exhibit sensitivity to the formulation adopted for the atmosphere's interaction with the land surface.

The atmosphere interacts with the terrestrial surface in three ways. First, there is the exchange of radiation between the two. Land surface albedo can vary widely, from about 0.09 to 0.60, over the earth's surface (see Dorman and Sellers 1989), and has a direct influence on the amount of shortwave (0.0–4.0 μm) radiation absorbed by the surface. Several GCM experiments have shown that alteration of the albedo alone may affect regional circulation. Charney et al. (1977), for example, suggested that an increased albedo in the Sahel region would give rise to reductions in the evapotranspiration rate, the cloudiness and the tropospheric moisture convergence, resulting in reduced rainfall.

A second influence of the land surface is the drag force exerted on the lowest layer of the atmosphere by the roughness elements, principally vegetation, projecting into the airflow. This drag force is a component of the turbulent exchange between surface and atmosphere, the intensity of which partly determines the rates of transfer of mass and heat. Sud et al. (1985) conducted GCM experiments in which the roughness of desert regions was changed from the standard value used for terrestrial surfaces (0.45 m) to the value used for the oceans (0.0002 m). This altered the convergence of horizontal water transport in the atmospheric boundary layer and resulted in large changes in the spatial distribution of convective precipitation.

† Work carried out while at NASA/GSFC on University of Maryland sponsored study leave from the NERC Institute of Hydrology, Wallingford, Oxon, United Kingdom.

Corresponding author address: Dr. Piers J. Sellers, COLA, Dept. of Meteorology, University of Maryland, College Park, MD 20742.

A third influence of the land surface on the atmosphere is through the availability of moisture for evapotranspiration and the control exerted by vegetation on its release. The radiant energy absorbed by the surface is partitioned into latent, sensible and storage heat. The ratio of these depends primarily on how the vegetation responds to environmental variables, particularly soil moisture, and partly on the rate of turbulent transport away from the surface. Shukla and Mintz (1982), Walker and Rowntree (1977) and others have shown that altering the regional soil moisture initialization may have large effects on the continental climates, particularly on precipitation rates.

All of the above sensitivity studies involved fairly gross changes in *individual* parameter values; for example, the study of Shukla and Mintz (1982) treated the terrestrial surface as completely saturated in their "wet case" and completely dry in their "dry case." Often these extreme specifications are not physically realistic, but such studies at least serve to illustrate that land surface processes may significantly affect the atmospheric circulation. Consequently, there is a need to simulate these processes realistically.

Most land surface parameterizations (LSPs) used in GCMs *independently* specify the reflectance, drag and energy partition properties for each model grid area, but in nature these three properties are closely interconnected by the type of vegetation present; see Sellers et al. (1986). The optical properties of the leaves, their size, number and geometric arrangement determine the surface reflectance and surface drag properties, and these, together with the vegetation physiology, also determine the vegetation's control on the evapotranspiration rate. The most self-consistent strategy for formulating an LSP is therefore to model the vegetation itself, and to calculate the reflectance, drag and energy partition in a mutually consistent way. The simple biosphere model (SiB) of Sellers et al. (1986), and the LSP of Dickinson (1984) attempt to do this.

SiB is a one-dimensional soil–vegetation–atmosphere model appended to the base of each GCM grid area. It represents the vegetation cover within a region by analogy with processes operating within a single representative plant, since more complex formulations explicitly recognizing several species would be computationally expensive.

SiB and the LSP of Dickinson (1984) contain only a limited number of vegetation types, which occur as extensive, uniform stands of identical morphology and physiology and may change discontinuously from one grid area to the next. Biologists, accustomed to the intricacy of species diversity and evolutionary ecology, often point out that there are a vast number of species within a given natural biome, all exhibiting complex interrelationships with each other and the environment. Conversely, it may be argued that there are influences which favor convergent evolution, in particular the pressure to optimize the probability of survival in a particular environment, which determine the form and function of the dominant vegetation in a natural biome with regard to energy interception and partition. Mori and Boom (1987) reported, for instance, that in the Amazon forest less than 14 percent of the vegetation species accounted for about half of the frequency of occurrence, density and bole cross-sectional area at a particular site; moreover, it was difficult to distinguish between leaves of different species on the basis of size or pigmentation because most were "simple mesophyll" leaves in the classification of Raunkaier (1934). Arguably, this similarity of form extends to similarity of function, at least in the context of photosynthesis and transpiration, with the species most responsible for energy processing converging on an optimal solution in the same environment. We do not, therefore, expect to observe, or have to model, the physiology of rare species within an averaged description.

The philosophy adopted in SiB is to exploit these simplifying assumptions and to consider each biome as composed of up to two layers of vegetation. Figure 1 shows the two layer structure of the SiB model, which consists of an upper-story canopy (trees or shrubs), whose variables are identified by the "c" subscript, and ground vegetation identified by a "g" subscript.

When bare or litter-covered soil contributes significantly to the energy and mass budget, a transfer pathway (subscript "s") is also defined. It is assumed that

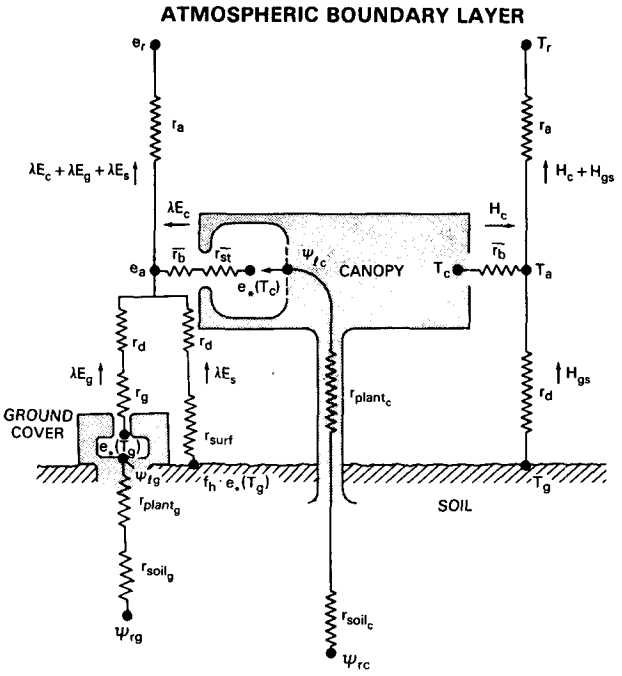

FIG. 1. Framework of the simple biosphere model (SiB). The transfer pathways for latent and sensible heat flux are shown on the left- and right-hand sides of the figure. The treatment of radiation and intercepted water has been omitted for clarity. Symbols are defined in Table 1.

the ground vegetation and soil surface share the same temperature which is denoted by the combined subscript "gs."

The purpose of SiB is to use the meteorological variables from the lowest layer of a GCM to calculate the fluxes of radiation, sensible heat, latent heat and momentum between the surface and the atmosphere. These calculated fluxes are returned to the overlying atmosphere and affect the subsequent development of the atmospheric circulation. SiB uses the variables given in Table 1a to calculate the fluxes given in Table 1b, while time-integrating eight prognostic variables given in Table 1c. [Note: Since Sellers et al. 1986, SiB has been modified to use the force-restore soil heat flux description of Deardorff (1978), which requires the deep soil temperature, T_d, as a prognostic variable.] In this study, SiB is used in the offline mode and the forcing variables are the micrometeorological measurements made 10 m above the forest canopy (see section 5a), while the calculated fluxes are compared to measured fluxes obtained 13 m above the canopy (see section 5c).

The model properties that determine how the meteorological forcing is transformed into calculated fluxes are determined by the prognostic variables in Table 1c together with the fairly large set of physical and physiological parameters in Table 2. These last parameters are used in a number of intermediate cal-

TABLE 1. Principal variables involved in SiB applications. The forcing variables, listed in Table 1a, are used to calculate fluxes which are returned to the atmosphere (see Table 1b). The calculated fluxes also determine the time rate of change of the model prognostic variables (see Table 1c), and the values of diagnostic variables (see Table 1d).

Symbol	Variable	Units
(a) Forcing variables		
T_r	air temperature at reference height	K
e_r	vapor pressure at reference height	mb
u_r	wind speed at reference height	m s^{-1}
$F_{v,\mu}$	visible (PAR) flux, solar beam component	W m^{-2}
$F_{v,d}$	visible (PAR) flux, diffuse component	W m^{-2}
$F_{n,\mu}$	near-infrared flux, solar beam component	W m^{-2}
$F_{n,d}$	near-infrared flux, diffuse component	W m^{-2}
$F_{t,d}$	thermal-infrared flux, all diffuse	W m^{-2}
P	precipitation rate	m s^{-1}
(b) Flux variables		
$F_{v,\uparrow}$	reflected visible flux	W m^{-2}
$F_{n,\uparrow}$	reflected near-infrared flux	W m^{-2}
$F_{t,\uparrow}$	upward longwave flux	W m^{-2}
λE	latent heat flux	W m^{-2}
H	sensible heat flux	W m^{-2}
τ	shear stress	kg m^{-1} s^{-2}
(c) Prognostic variables		
T_c	upper-story canopy temperature	K
T_{gs}	ground surface temperature	K
T_d	deep soil temperature	K
M_c	upper-story interception water storage	m
M_g	ground cover interception water storage	m
W_1	surface soil moisture wetness	
W_2	root zone soil moisture wetness	
W_3	recharge zone soil moisture wetness	
(d) Diagnostic variables: (Resistance, flux and potential variables)		
λE_c, λE_g, λE_s	canopy, groundcover and soil latent heat fluxes	W m^{-2}
H_c, H_{gs}	canopy, ground sensible heat fluxes	W m^{-2}
r_a	aerodynamic resistance between canopy air space and reference height, z_r	s m^{-1}
r_b	canopy bulk boundary layer resistance	s m^{-1}
r_d	aerodynamic resistance between ground and canopy air space	s m^{-1}
r_c	area-averaged canopy (stomatal) resistance	s m^{-1}
r_g	ground cover (stomatal) resistance	s m^{-1}
r_{surf}	bare soil surface resistance	s m^{-1}
ψ_l, ψ_r	leaf, root zone moisture potentials	m
T_a, e_a	air temperature, vapor pressure in canopy air space	K, mb

TABLE 2. SiB parameter set for the tropical forest biome. Column I lists the preliminary data set described by Willmott and Klink (1986). Column II lists the adjusted initial set combined with the literature review physiological parameters. Note that no parameter values have been specified for the ground cover, as this is assumed to be negligible.

Symbol	Definition	Units	I	II
(a) Morphological parameters				
V_c	fractional area covered by upper-story canopy		0.7	0.98
χ_L	leaf angle distribution factor		—	0.1
z_2	height of canopy top	m	35.0	35.0
z_1	height of canopy base	m	19.0	1.0
z_c	height of maximum canopy density	m	—	28.2
L_{tc}	canopy leaf area index	$m^2\ m^{-2}$	10.0	8.0
z_d	rooting depth	m	1.0	1.0
D_d	root length density	$m\ m^{-3}$	10 000.	20 000.
D_1	thickness of the three soil moisture storage layers	m	—	0.02
D_2		m	—	0.98
D_3		m	—	1.00
(b) Physiological parameters				
N_c	green leaf fraction		—	0.95
a	light dependent stomatal	$J\ m^{-3}$	56 661.2	4765.0
b	response parameters	$W\ m^{-2}$	12.8	16.5
c		$s\ m^{-1}$	250.0	33.0
T_L	lowest, highest and optimum temperatures for stomatal functioning; see Eq. (11)	K	—	273.0
T_h		K	—	318.0
T_0		K	—	303.0
h_5	parameter governing stomatal response to the atmospheric water vapor pressure; see Eq. (13)	mb^{-1}	—	0.0222
ψ_{c_1}	parameters that specify leaf water potential dependency of stomatal functioning; see Eq. (12)	m	—	−200.0
ψ_{c_2}		m	—	−300.0
r_{plant}	resistance imposed by plant vascular system	s	—	2.45E8
R	root resistance per unit length	$s\ m^{-1}$	—	7.50E12
(c) Physical parameters				
$\alpha_{(v,L)}$	visible live leaf reflectance		0.05	0.05
$\alpha_{(v,D)}$	visible dead leaf reflectance		—	0.36
$\alpha_{(n,L)}$	near-infrared live leaf reflectance		0.40	0.45
$\alpha_{(n,D)}$	near-infrared dead leaf reflectance		—	0.58
$\tau_{(s,L)}$	visible live leaf transmittance		0.10	0.10
$\tau_{(v,D)}$	visible dead leaf transmittance		—	0.22
$\tau_{(n,L)}$	near-infrared live leaf transmittance		0.55	0.25
$\tau_{(n,D)}$	near-infrared dead leaf transmittance		—	0.38
$\alpha_{s(v)}$	visible ground reflectance (litter)		—	0.11
$\alpha_{s(n)}$	near-infrared ground reflectance (litter)		—	0.225
	leaf width	m	0.07	0.05
	leaf length	m	0.17	0.10
z_{gs}	ground roughness length	m	—	0.05
θ_s	soil pore space	$m^3\ m^{-3}$	0.458	0.458
ψ_s	soil moisture potential at saturation	m	−0.198	−0.198
K_s	saturated soil hydraulic conductivity	$m\ s^{-1}$	3.5E-6	3.5E-6
B	soil moisture potential parameter		7.797	7.797

culations, some performed offline, to calculate the radiative transfer properties of the surface and the values of three aerodynamic resistances; r_a, $\overline{r_b}$ and r_d, and three surface resistances, $\overline{r_c}$, r_g and r_{surf}; see Fig. 1.

Sellers and Dorman (1987) performed a number of sensitivity studies using SiB and concluded that the model was insensitive to many of the morphological parameters in Table 2, but that transpiration from tall vegetation was sensitive to those parameters controlling the canopy resistance, $\overline{r_c}$. All the parameters listed in Table 2 must be assigned values prior to the operation of SiB and initially these were specified from the ecological and geographical literature; see Willmott and Klink (1986). Here we test an alternative method of

specification which involves optimizing the model output against measured fluxes by iteratively changing a critical subset of input parameters.

This paper reports a calibration of the tropical forest biome. SiB was calibrated using a unique set of point micrometeorological and hydrological data gathered over a two year period at an experimental site over undisturbed natural forest in the central Amazon basin. The parameters derived here are those which, on average, best describe the experimental data regardless of the season in which they were collected. It is later shown that there is a seasonal difference between the latent heat flux, calculated with these average parameters, and the measured evapotranspiration, which is significant at the 10 percent level.

2. The tropical forest biome as represented in SiB

The structure and formulation of SiB has been described in detail in Sellers et al. (1986), and tested in Sellers and Dorman (1987): the complete details are not reproduced here. This section reviews the parameters used in SiB to describe the tropical forest (TF) biome and discusses how they are applied to describe energy and mass transfer.

a. Tropical forest parameter set

Table 2, column I gives the parameters originally prescribed by Willmott and Klink (1986) for this biome. A literature review and some field observations suggested some alterations and additions to give the parameters in Table 2, column II. The salient features of this basic parameter set are as follows: the canopy extends from 1 m (z_1) above the soil to 35 m (z_2) with an assumed maximum density at 28.2 m (z_c) (80 percent of the difference between z_1 and z_2). The leaf area index is 8.0, while 98 percent of the vegetation *area* exposed above ground is assumed to be green. The rooting depth extends down to 1 m, with root physical and physiological properties taken from Jordan and Escalante (1980) and Federer (1979), respectively, these last being derived from data for deciduous trees in the eastern United States.

The optical and physiological properties of the leaves were initially drawn from the data described by Willmott and Klink (1986). In the absence of better values, the optical properties of the ground were arbitrarily assigned by assuming that it was covered with a layer of horizontal dead leaves, using data from Strebel (personal communication).

Since energy partition in forest biomes is particularly sensitive to stomatal control, a brief ecological literature review was undertaken to update the physiological parameters previously defined as representative of the TF biome by Willmott and Klink (1986). Appendix B summarizes the results and itemizes sources. An average parameter set was defined as the composite of these sources and is hereafter referred to as the literature review parameter set, see Table 3, column I. Additionally, Pearcy (1987) proposed a substantially different set of stomatal coefficients based on data gathered in an Australian tropical forest biome, which is presented in Table 3, column II. The optimization procedure described later provided a third set of parameters (Table 3, column III) which gives the best match between simulated and measured heat fluxes. These three sets of stomatal coefficients and the time-series of canopy resistance values they produce in simulation are compared to analyses of in situ measurements of stomatal resistance obtained by Roberts et al. (1988); see Table 3, column IV.

Although inherently one-dimensional, the SiB model recognizes certain two-dimensional features. In particular, there may be discrete gaps in both upper and lower canopies, with fractional canopy cover V_c and V_g, respectively. These gaps are assumed to be randomly and independently distributed. In the TF biome, only the fractional canopy cover V_c is relevant: it refers to the occurrence of large scale gaps in the canopy, so that direct radiation penetration is independent of solar angle. The canopy cover for tropical forest is more usually penetrated with smaller holes, typically 1 m^2

TABLE 3. Physiological parameter sets for SiB; see Table 2 for explanation of symbols. The literature review values were obtained from a variety of sources as described in appendix B. The Pearcy parameter set is based on the literature review parameter set but with values of *a*, *b*, *c* and h_5 obtained from analyses of the data of Pearcy (1987); see Appendix B. The Roberts et al. parameter set is based on the optimized parameter set (see section 4d) with *a*, *b* and *c* drawn from analyses of the data of Roberts et al. (1989); see appendix B.

Parameter	I Literature review	II Pearcy	III Optimized	IV Roberts et al.
a	4765.0	3525.3	2335.9	2926.0
b	16.5	0.00	0.0145	0.0
c	33.0	131.3	153.5	126.2
h_5	0.0222	0.0226	0.0273	0.0273
ψ_{c_1}	−200.0	−200.0	−15.22	−15.22
ψ_{c_2}	−500.0	−500.0	−1553.50	−1553.50
R	20 000.	20 000.	5122.3	5122.3
L_{t_c}	8.0	8.0	5.01	5.01
N_c	0.98	0.98	0.905	0.905

or less. Measured values of V_c, made for instance with an anascope, are typically 0.92 (Lloyd and Marques 1988) and are probably realistic in the description of direct canopy penetration by precipitation or overhead solar radiation but are likely to be an underestimate of the effective canopy cover in a model which treats radiation dynamics in one dimension (Sellers et al. 1986; and Sellers 1985). Perhaps a more realistic estimate of the effective value of V_c is 0.98, which is based on the observation that the solar radiation measured beneath the canopy is only about 2 percent of that above (Shuttleworth et al. 1984b). This value is used throughout the present analysis.

In SiB, soil evaporation is assumed to occur from a shallow surface layer, 0.02 m deep, and to be controlled by an empirically defined soil surface resistance. The adequacy or otherwise of this aspect of the model cannot be tested in the present calibration, since energy exchange with the soil plays a very minor role in the TF biome (Shuttleworth et al. 1984b). Equally, the assumption implicit in the SiB model, that surface water movement and storage are not important features of land surface energy partition, cannot be tested with these data, since they refer to "terra firma" tropical forest, which has extremely high surface and subsurface infiltration rates. The SiB model therefore performs realistically in this case, with almost all the rainfall immediately entering the soil and ultimately generating runoff by gravitational drainage and hydraulic diffusion, initially through the root zone, and then through an underlying recharge layer.

Large areas of the Amazon forest around the river and its major tributaries undergo extensive and regular flooding as river levels rise seasonally. In practice, the consequences of this on the spatial variability of surface energy partition are likely to be less significant than they may appear. The continued presence of a high leaf area index means that most of the energy interception, and most of the control of the energy partition, remains in the forest canopy. The direct removal of an effective soil surface resistance has little effect on total canopy evaporation at high leaf area indexes (Shuttleworth and Wallace 1985). The indirect effect of the spatial variability in soil moisture, i.e., through soil water tension on stomatal control, is moderated by the fact that water is usually freely available in the soil of the more extensive terra firma portions of the forest in any case (Shuttleworth 1988).

The next three sections describe how the parameters in Table 2 are used to calculate the radiative transfer (surface reflectance), turbulent transport (drag and aerodynamic resistances) and energy partition (biophysical control via surface resistance) properties of the TF biome.

b. *Radiative transfer*

The description of radiative transfer in SiB has been reported by Sellers (1985) and Sellers et al. (1986). This section provides an overview of the methods and assumptions involved.

Each vegetation layer is assumed to have a uniform greenness fraction throughout its depth, and has leaves randomly arranged in space within its specified fractional cover. Live leaves are assumed to have the one set of optical properties (scattering coefficient, reflectance and transmittance), and dead leaves another. The radiant spectrum is split into three portions, visible ($0.4 < \lambda < 0.7$ μm), near-infrared ($0.7 < \lambda < 4$ μm) and thermal infrared ($\lambda > 4$ μm); and mean optical properties are assigned to the leaves over these wavelength intervals as the weighted average of the dead and live components. It is assumed that the visible radiation is directly equivalent to photosynthetically active radiation (PAR).

The radiative transfer submodel uses the two-stream approximation formulation described by Ross (1975), Meador and Weaver (1980), Dickinson (1983) and Sellers (1985). Divergence equations are used to describe the interaction of the vegetated surface with direct beam and diffuse visible and near-infrared radiation within the canopy. These equations and their solutions are given in Sellers (1985).

The analytical solution of the equation set yields the upward radiation fluxes at the top of the upper-story canopy which are summed to give reflected solar radiation flux. The relative fractions of radiation absorbed by the upper-story canopy and the ground cover are also calculated. All of the above radiative transfer properties depend on the optical properties of the vegetation and soil, and the number and geometrical arrangement of the leaves and stems.

The exchange of longwave radiation is calculated using the canopy and ground temperature in the Stefan–Boltzmann equation; it is assumed that all of the downward thermal infrared flux is diffuse.

c. *Turbulent transport*

The aerodynamic resistance pathway is shown in Fig. 1. There are three resistances: r_d, the resistance between the soil surface (and ground cover, if any) and the canopy air space; $\overline{r_b}$, the resistance between all of the canopy leaves and the canopy air space; and r_a, the resistance between the canopy air space and the reference height, z_r. In a GCM, z_r is located within the lowest model layer. In the present exercise, z_r is the measurement height for the air temperature, T_r, vapor pressure, e_r, and wind speed, u_r, and is 45 m.

Sellers et al. (1986) described a methodology for computing r_d, $\overline{r_b}$ and r_a from the morphological parameters given in Table 2. This original formulation represented the upper-story canopy as a constant density, porous block of material extending from the canopy base, z_1, to the canopy top, z_2. A turbulent transition layer was assumed to extend from z_2 to a specified height z_m above the canopy, above which the log–linear

wind profile was considered valid. Between z_m and the top of the canopy the shear stress was assumed constant but the relationship between the momentum transfer coefficient, K_m, and the extrapolated log–linear value was empirically adjusted to be consistent with the data of Garratt (1978).

Within the canopy the leaves absorb momentum from the local airflow so that the shear varies with height as

$$\frac{\partial \tau}{\partial z} = \rho \frac{C_d \overline{L_d}}{p_s} u^2 \quad (z_1 < z < z_2) \tag{1}$$

and

$$\tau = \rho K_m \frac{\partial u}{\partial z} \quad (z > z_1), \tag{2}$$

where τ is the shear stress (kg m^{-1} s^{-2}); ρ is the air density (kg m^{-3}); z is height (m); C_d is the leaf drag coefficient; p_s is the leaf shelter factor, see Sellers and Dorman (1987); $\overline{L_d}$ is the area-averaged leaf area density (m m^{-2}); u is the local wind speed (m s^{-1}); and K_m is the momentum transfer coefficient (m^2 s^{-1}).

It is assumed that K_m is a function of the local wind speed in the canopy air space such that

$$K_m = \sigma u \quad (z_1 < z < z_2), \tag{3}$$

where σ is a constant determined from solution of momentum balance equations (m), z_1 is the height of canopy base (m), and z_2 is the height of canopy top (m).

Some of the momentum entering the canopy is absorbed following Eq. (1) with the remainder being absorbed at the ground according to

$$\tau = \rho C_{D_{gs}} u^2, \quad (z = z_1), \tag{4}$$

where $C_{D_{gs}}$ is the ground drag coefficient, which equals $[k/\ln(z_1/z_{gs})]^2$; and z_{gs} is the ground roughness length (m).

The zero plane displacement height is calculated from a modification of the expression of Thom (1971) whereby

$$d = \frac{\int_{z_1}^{z_2} u^2 z dz}{\int_{z_1}^{z_2} u^2 dz + \frac{\tau}{\rho}\Big|_{z_1} \frac{p_s}{\overline{L_d} C_d}}, \tag{5}$$

where d is the zero plane displacement (m).

Equations (1) to (5) can be solved in combination with the modified log–linear, above-canopy description, see Sellers et al. (1986), to yield values of z_0, d and the profiles of K_m and u given the input parameters z_2, z_1, C_d, p_s, $\overline{L_d}$ and z_{gs} and two empirical parameters, G_1 and G_2, which were used to modify the wind and momentum transfer profile above the canopy. It was originally assumed that the leaf area density, L_d, was distributed evenly between z_1 and z_2, which greatly facilitates the solution process. The various resistances are then obtained by

$$\overline{r_b} = \int_{z_1}^{z_2} \frac{p_s C_s}{\overline{L_d}\sqrt{u}} dz = \frac{C_1}{\sqrt{u_2}} \tag{6}$$

$$r_d = \int_{z_{gs}}^{h_a} \frac{1}{K_s} dz = \frac{C_2}{u_2}, \tag{7}$$

where K_s is the heat/vapor transfer coefficient, assumed to be equal to K_m, m^2 s^{-1}, h_a is the canopy source height (m) obtained from solution of (1) through (5); C_s is the leaf transfer coefficient (see Sellers and Dorman 1987); u_2, u_r are the wind speeds at z_2 and z_r, respectively, (m s^{-1}); and C_1, C_2 are constants obtained from (6) and (7). The constants, C_1, C_2, z_0, d and h_a are calculated just once for each set of vegetation morphological parameters prior to a SiB simulation run. Equations (6) and (7) hold under neutral conditions. Simple corrections are made to these formulae in non-neutral conditions (see Sellers et al. 1986).

Applying the above procedure to the morphological parameters listed in Table 2 yielded the aerodynamic parameters listed in Table 4, column I and a calculated neutral value of u_*/u_r, which did not compare well with the observations of Shuttleworth et al. (1984a);

TABLE 4. Canopy aerodynamic properties as calculated by two versions of the SiB turbulent transfer (preprocessor) package. Column I refers to results produced with the original constant foliage density description of Sellers et al. (1986); note high values of z_0 and u_*/u_r. Columns II and III list results obtained with new procedure (see appendix A). Column II shows a predicted neutral value of u_*/u_r in better agreement with the average value reported by Shuttleworth et al. (1984a) of about 0.175. Columns I and II assume a canopy leaf area index of 8.00. Column III shows the impact of reducing L_{ic} to 5.01 (in accordance with the results from the optimization procedure) in the new package. There is relatively little difference in z_0, d and u_*/u_r between columns II and III.

Symbol	Variable	Unit	I	II	III
L_{ic}	Leaf area index	(m^2 m^{-2})	8.00	8.00	5.01
z_0	Roughness length	m	4.49	2.02	2.36
d	Zero plane displacement	m	27.84	28.81	27.37
C_1	$\overline{r_b}$ coefficient	(s m^{-1})$^{1/2}$	4.38	5.59	7.22
C_2	r_d coefficient	—	463.55	1177.14	503.13
h_a	Canopy source height	m	22.53	24.81	24.02
u_*/u_r	Friction velocity divided by wind speed at reference height	—	0.306	0.197	0.204

see later sections. This result suggests that the calculated value of $(z_r - d)/z_0$ was too low.

The procedure seems to work well with short dense vegetation (Sellers and Dorman (1987), but the results of Shaw and Pereira (1982) indicate that the assumption of a constant leaf area density with height might give rise to errors when applied to tall canopies. The turbulent transfer description was extended to allow for a triangular distribution of leaf area density with a height of maximum leaf area density, z_c, and linear decreases in density above and below this. The equations for the leaf area density are then

$$\overline{L_d} = a_1 + b_1 z \quad (z_1 < z < z_c)$$
$$\overline{L_d} = a_2 + b_2 z \quad (z_c < z < z_2). \qquad (8)$$

Substitution of (8) into (1) and (7) yields a description of the height-dependent variation in u between z_1 and z_2 in terms of Bessel functions (see appendix A). In the course of this reformulation, the link between the within-canopy profiles of u and K_m with their counterparts above the canopy was also changed so as to optimize the results produced by this description against those produced by the second order closure model of Shaw and Pereira (1982) (see appendix A). The resulting formulation describes continuous profiles of u and K_m (or K_s) which are then integrated to yield $\overline{r_b}$, r_d and r_a. The new values of z_0, d, C_1, C_2, h_a and u_*/u_r are given in Table 4, columns II and III and are later demonstrated to provide a substantially better fit to observations of u_* and wind speed profiles in the upper half of the canopy. The revised values are used throughout the remainder of this analysis and the revised turbulent transfer model (described in appendix A) has now been incorporated into SiB.

d. Biophysical control of evapotranspiration

Some modifications to the original surface resistance calculations of Sellers (1985) and Sellers et al. (1986) have already been discussed in Sellers and Dorman (1987).

As shown in Fig. 1, three surface resistances are used in SiB: r_{surf}, r_g and $\overline{r_c}$. The soil surface resistance, r_{surf}, governs moisture flux from the top, thin (0.02 m) soil layer to the overlying air and was defined following the empirical expression of Shu Fen Sun (1982),

$$r_{\text{surf}} = d_1 + d_2(W_1)^{-d_3}, \qquad (9)$$

where d_1, d_2, d_3 are empirical constants obtained from data, equalling 30, 3.5, 2.3, respectively.

In this study, the soil evaporation is relatively small and the validity or otherwise of this expression cannot be tested.

Transpiration from the (upper-story) vegetation and evaporation of intercepted rainfall are the dominant processes controlling energy partition in a tropical forest. SiB treats this upper story as a single species, whose behavior is assumed representative of all the vegetation in the biome. The surface resistances of vegetation in SiB, are set equal to the parallel summation of the component stomatal resistances as described in Sellers (1985). In this way, the two vegetation resistances, r_g and $\overline{r_c}$, represent the combined resistances of all of the leaves in the ground cover (here taken to be practically nonexistent) and the upper-story canopy, respectively. They are obtained by integrating functions describing the dependence of individual leaf stomatal resistances upon PAR flux density over all leaf azimuth and inclination angles and from the top to the bottom of the canopy. The effects of leaf temperature, leaf water potential and air vapor pressure deficit are assumed to apply uniformly throughout each canopy and are applied as multiplicative factors to the light-integrated portion of the canopy resistance.

The integration scheme assumes an expression for the stomatal resistance of an individual leaf following Jarvis (1976),

$$r_s = \left[\frac{a}{b + \mathbf{F}_\pi \cdot \mathbf{n}} + c\right][f(T_c)f(\psi_l)f(\delta e)]^{-1}, \qquad (10)$$

where r_s is the individual green leaf stomatal resistance, (s m^{-1}) a, b, c are species-dependent PAR response constants (J m^{-3}, W m^{-2}, s m^{-1}); $\mathbf{F}_\pi$ is a PAR flux density vector (W m^{-2}), equaling F_v in this application; $\mathbf{n}$ is the leaf normal vector; and $f(T_c), f(\psi_l), f(\delta e)$ are adjustment factors for temperature, leaf water potential and vapor pressure deficit.

The factors $f(T_c), f(\psi_l)$ and $f(\delta e)$ vary from unity, under optimal conditions, to zero when transpiration is totally suppressed by adverse environmental conditions. They are specified following Jarvis (1976), apart from $f(\psi_l)$, which is specified following Choudhury (1983). Thus

$$f(T) = h_3(T - T_1)(T_h - T)^{h_4} \quad (0 \leqslant f(T) \leqslant 1), \qquad (11)$$

where $h_3 = 1/(T_0 - T_1)(T_h - T_0)^{h_4}$, $h_4 = (T_h - T_0)/(T_0 - T_1)$, and T_1, T_h, T_0 are the lowest, highest and optimum temperatures for transpiration (K);

$$f(\psi_l) = \frac{\psi_l - \psi_{c_2}}{\psi_{c_1} - \psi_{c_2}} \quad (0 \leqslant f(\psi_l) \leqslant 1) \qquad (12)$$

where ψ_l is leaf water potential (m) and ψ_{c_1}, ψ_{c_2} are the values of ψ_l when stomata start to close and are completely closed, respectively (m); and

$$f(\delta e) = 1 - h_5 \delta e, \quad 0 \leqslant f(\delta e) \leqslant 1, \qquad (13)$$

where δe is vapor pressure deficit (mb), h_5 is a species-dependent constant (mb^{-1}).

The expression for individual leaf stomatal resistance, (10), may be rewritten as

$$r_s = f(\mu_\pi, \xi, \theta, F_\pi)f[\textstyle\sum]^{-1}, \qquad (14)$$

where F_π is PAR flux density (W m^{-2}), μ_π is the cosine of PAR flux zenith angle, and θ, ξ are the leaf inclination and azimuth angles, and in which $f(\mu_\pi, \xi, \theta, F_\pi)$, represents the interaction of leaf angle with PAR flux and $f(\sum)^{-1}$ is given by

$$f[\sum] = f(T)f(\psi_l)f(\delta e), \quad (0 < f(\sum) < 1). \quad (15)$$

Since $f[\sum]$ is assumed to be uniform throughout the canopy, determining the surface resistances reduces to integrating the light dependent part of Eq. (14). For the upper-story canopy, the surface resistance, $\overline{r_c}$, is thus given by

$$\frac{1}{\overline{r_c}} = V_c N_c f[\sum] \times \int_0^{L_t}\int_0^{\pi/2}\int_0^{2\pi} \frac{0(\xi,\theta)}{r_s(\mu_\pi, \xi, \theta, F_s)} \mathrm{Sin}\theta d\xi d\theta dL, \quad (16)$$

where V_c is the cover fraction of the upper-story canopy, N_c is the fraction of green photosynthesizing leaves, L_t is the leaf area index of the upper-story canopy, and $0(\xi, \theta)$ is the leaf angle distribution function. Two additional adjustment terms appear in Eq. (16). The first, V_c, is the grid-area-average of the fractional area covered by the upper-story canopy; the second, N_c, is the fraction of live leaves present. In SiB, the presence of dead leaves in a canopy is assumed to affect average canopy conductance directly; leaves are assumed to be either alive and fully active or dead with infinite stomatal resistance. The dead leaves are further assumed to be equally distributed throughout the canopy. In this way the effect of canopy greenness is represented by a single multiplicative constant, N_c (in the range 0 to 1), acting on the integrated dry canopy conductance. The average value of N_c is not strictly significant when the model parameters are determined by calibration against field data, *providing* this value is the same both in calibration and operation.

The analytical solutions to Eq. (16) for different leaf angle distributions were given by Sellers (1985). The complex leaf angle integrations, however, are avoided in SiB by defining a mean leaf projection, $G(\mu_\pi)$, for a given incoming PAR flux direction, μ_π, so that Eq. (16) simplifies to

$$\frac{1}{\overline{r_c}} = V_c N_c f(\sum) \int_0^{L_t} \frac{G(\mu_\pi)}{r_s(\mu_\pi, F_\pi, G(\mu_\pi))} dL, \quad (17)$$

where $G(\mu_\pi)$ is the semi-empirical formulation of Goudriaan (1977) which defines the canopy leaf projection for a given zenith direction, μ, as

$$G(\mu) = \phi_1 + \phi_2\mu, \quad (18)$$

where $\phi_1 = 0.5 - 0.633\chi_L - 0.33\chi_L^2$, $\phi_2 = 0.877(1-2\phi_1)$, χ_L is the Ross (1975) leaf angle distribution function, which equals $\pm\int_0^{\pi/2}|1 - 0(\theta)|\sin\theta d\theta$. χ_L is equal to +1 for horizontal leaves, 0 for a spherical leaf angle distribution, −1 for vertical leaves and $0(\theta)$ = leaf angle distribution function defined as a function of θ only. In Eqs. (16) and (17), the flux of PAR, F_π, has to be specified as a continuous function of L using the semi-empirical expression of Goudriaan (1977) whereby

$$F_{\pi(L)} = F_{\pi(0)}e^{-\kappa \mathrm{L}}$$

$$\kappa = \frac{G(\mu_\pi)}{\mu_\pi}(1 - \omega_\pi)^{1/2}, \quad (19)$$

in which $F_{\pi(0)}$, $F_{\pi(L)}$ are PAR fluxes above and at level L within the canopy, respectively (W m^{-2}), and ω_π is the leaf scattering coefficient for PAR. The solution of Eq. (17) with (18) and (19) yields an analytical expression for surface resistance:

$$\frac{1}{\overline{r_c}} = \frac{V_c N_c}{\kappa c} F[\sum]\left[\frac{b}{fF_{\pi(0)}} \ln\left\{\frac{\mu_\pi f e^{-\kappa \mathrm{L}t} + G(\mu_\pi)}{\mu_\pi f + G(\mu_\pi)}\right\} - \ln\left\{\frac{\mu_\pi f + G(\mu_\pi)e^{-\kappa \mathrm{L}t}}{\mu_\pi f + G(\mu_\pi)}\right\}\right], \quad (20)$$

where

$$f = \frac{a + bc}{cF_{\pi(0)}}.$$

In this way, the canopy resistance, $\overline{r_c}$, is defined as an explicit function of the environmental variables and vegetation parameters during routine operation.

The dependence of stomatal resistance on leaf water potential, through the function $f(\psi_l)$ in Eqs. (12) and (17) is the mechanism whereby transpiration responds to soil water availability and the evaporative demand of the atmosphere. The extent and duration of soil water deficit in the TF biome, where rainfall is heavy and frequent, is not large, and the calibration of this particular aspect of SiB has only limited stringency in the present study. On the other hand, transpiration flux is high during dry days and a significant daily cycle in leaf water stress develops to maintain it. Calibration of this aspect of the model was possible using the leaf water potential data of Roberts et al. (1989).

In SiB, the leaf water potential is calculated as a function of the soil moisture potential plus the additional potential required to raise the transpiration flux against gravity and across the diffusion resistances encountered in the stem, the roots and the soil surrounding the roots. This simple hydraulic analogue follows the catenary models of van der Honert (1948) and Federer (1979). Recent work by Davies et al. (1986) and others suggests that root hormones contribute to the relationship between stomatal resistance and soil moisture stress. Pending an improved formulation to model this, however, SiB retains a catenary description of the process as described in Sellers et al. (1986).

The leaf water potential, ψ_l, is calculated from the equation

$$\psi_l = \psi_r - z_T - \frac{E_d}{\rho_w}[\overline{r_{\mathrm{plant}}} + \overline{r_{\mathrm{soil}}}], \quad (21)$$

where ψ_r is the soil moisture potential in the root zone (m); z_T is the height of transpiration source (m), which equals h_a for the canopy (m); E_d is the transpiration rate (kg m^{-2} s^{-1}); ρ_w is the density of water (kg m^{-3}); $\overline{r_{\text{plant}}}$ is area-averaged plant resistance (s); and $\overline{r_{\text{soil}}}$ is area-averaged root and soil resistance (s). The soil moisture potential in the root zone is calculated by summing the empirical expression of Clapp and Hornberger (1978) over the soil layers, thus

$$\psi_r = \frac{\psi_s}{z_d} \sum_0^{z_d} D_i W_i^{-B}, \tag{22}$$

where D_i is the depth of ith layer (m), z_d is the rooting depth (m), ψ_s is soil moisture potential at saturation (m), W is soil moisture fraction of ith layer, and B is an empirical parameter.

The soil and root resistance, $\overline{r_{\text{soil}}}$ is taken as a function of root density and resistance properties, soil texture and soil moisture content following Federer (1979):

$$\overline{r_{\text{soil}}} = (R/D_d + \alpha_f/K_r)/z_d \tag{23}$$

with

$$\alpha_f = \frac{1}{8\pi D_d}\left[V_r - 3 - 2\ln\left(\frac{V_r}{1 - V_r}\right)\right],$$

where R is resistance per unit root length (s m^{-1}), D_d is root density (m m^{-3}), V_r is volume of root per unit volume of soil, and K_r is mean soil hydraulic conductivity in the root zone (m s^{-1}). Soil hydraulic conductivity in the root zone, K_r, is obtained by manipulation of the expressions of Clapp and Hornberger (1978) and Milly and Eagleson (1982) which yields K_r as a function of ψ_r, thus

$$K_r = K_s\left(\frac{\psi_s}{\psi_r}\right)^{(2B+3)/B}, \tag{24}$$

where K_s is saturated hydraulic conductivity (m s^{-1}). The transpiration rate from the dry part of the canopy, E_{dc}, (λE_c in Fig. 1) is then given by

$$\lambda E_{dc} = \left[\frac{e^*(T_c) - e_a}{\overline{r_c} + \overline{r_b}}\right]\frac{\rho c_p}{\gamma}(1 - W_c), \tag{25}$$

where W_c is the wet fraction of the canopy.

Study of Eqs. (10)–(25) reveals that the canopy transpiration rate, E_{dc}, is a function of both the atmospheric forcing variables (the evaporative demand), and the supply of soil moisture. Surface resistance is the regulating link and is controlled by both demand and supply through ψ_l; see Eqs. (12), (15), (20), and (25). The technique used to solve these equations is described in Sellers et al. (1986) and Sellers and Dorman (1987). Since ground cover in the tropical forest biome is assumed to be negligible, further discussion of r_g is omitted here: in other circumstances it is computed in the same way as $\overline{r_c}$.

Table 3 shows the values of the various physiological constants governing leaf stomatal resistance as obtained from curve fits to data obtained from the literature review, Pearcy (1987), the optimization procedure and the data of Roberts et al. (1989) (see later sections). The light response portions of these curves are shown in Fig. 2. The simulations will show that the range of responses depicted in Fig. 2 will have marked effects on the predicted energy balances. Further details on the origin of these parameters may be found in ap-

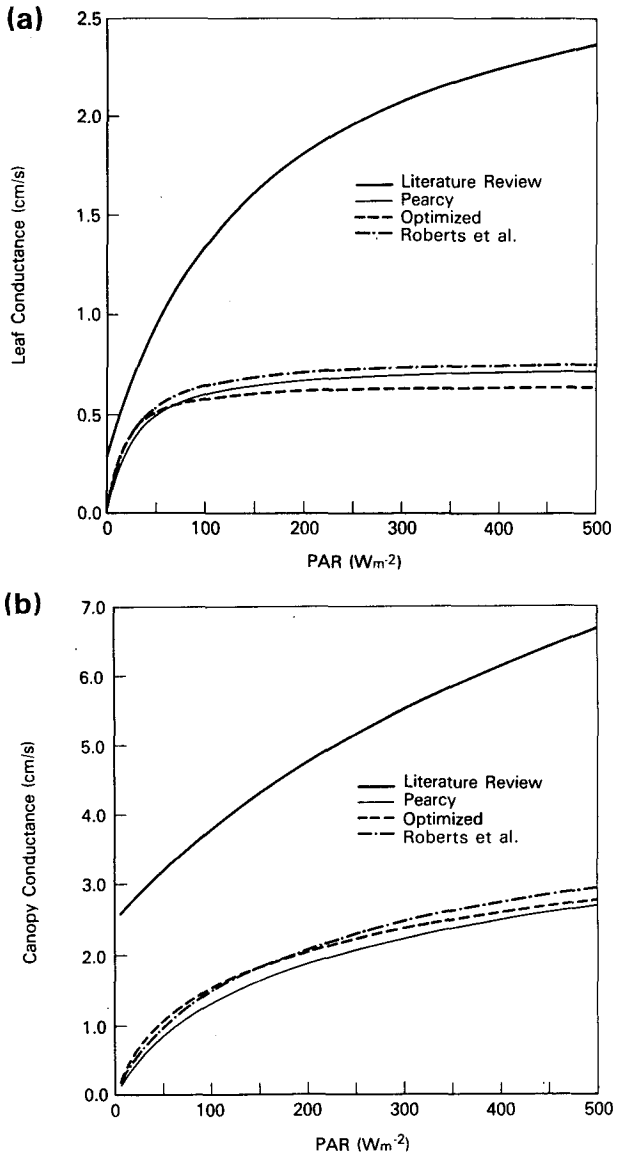

FIG. 2. (a) Light dependent (unstressed) leaf stomatal conductance functions ($1/r_s$) as calculated from the literature review, Pearcy, optimized and Roberts et al. parameter sets for a, b and c; see Table 3. (b) The same parameters are used to calculate the light dependent (unstressed) canopy conductance values ($1/\overline{r_c}$) for a canopy of leaf area index = 8.0, χ_L = 0.1 and a vertical PAR flux. Note how the variation of canopy conductance with PAR flux is more linear than that of individual leaf conductance; discussed in Sellers (1985).

pendix B. (N.B. For greater clarity, all figures showing stomatal conductance use units of cm s^{-1} rather than m s^{-1}).

All of the previous discussion refers to the canopy conductance in dry conditions. In practice, the presence of surface water on the vegetation can dramatically alter evaporation rates from forest canopies; see for example Shuttleworth and Calder (1979).

The submodel used in SiB to describe rainfall interception by the two vegetation stories is conceptually similar to that described by Rutter et al. (1971) as modified by Hancock et al. (1983), but incorporates simplifying assumptions to enhance operational efficiency. In particular, the evaporation of water stored on the tree stems would require the maintenance of two additional prognostic variables, and is rarely found to contribute more than a few percent to total interception loss in more complex models. This process is not given separate representation in SiB, rather it is assumed to be incorporated into a description which envisages two water stores, one for each vegetation story. The status of each of these water stores are maintained as prognostic variables in the model, M_c and M_g.

The upper-story canopy is filled by incoming precipitation, while the ground cover store is filled by throughfall from the vegetation above. The throughfall has two components, the first is when the incoming water passes directly through the (large scale) gaps in the two storys, i.e., $(1 - V_c)$ and $(1 - V_g)$, and the second is when the water passes directly through small scale gaps, in a manner analogous to light extinction by a canopy of totally black leaves; see Sellers et al. (1986). The model assumes that no drainage occurs from either story until the water storage reaches a critical saturation level, at which stage excess water is assumed to drain immediately.

In the TF biome, where only the upper-story vegetation is represented, the SiB model computes upper-story interception loss by

$$\lambda E_{wc} = \left(\frac{e_*(T_c) - e_a}{\overline{r_b}}\right)\frac{\rho c_p}{\gamma}\cdot W_c, \qquad (26)$$

where λE_{wc} is upper-story canopy interception loss rate (W m^{-2}); W_c is wetted fraction of the canopy, equaling M_c/S_c; M_c is canopy interception storage (m); and S_c is the maximum value of M_c (m).

Prior to this study, S_c was calculated by assuming that the canopy could hold 0.25 mm of water for each unit leaf area, following the work of Hancock and Crowther (1979) on Sitka spruce. The present data suggests that the *TF* canopy can hold only 0.1 mm of water per unit leaf area.

3. Experimental systems and site location

Previous and parallel publications provide details of the experimental site, instrumentation, data collection and analysis procedures, see Shuttleworth et al. (1984a), Moore (1986), Lloyd and Marques (1988), and Shuttleworth (1988). These are reported here only in overview, together with comments on the data reliability and estimated errors where they influence the quality of the present calibration.

The experimental site was in terra firma forest located in the Reserva Florestal Ducke, 25 km from Manaus, Amazonas Brazil (latitude 2°57′S, longitude 59°57′N) at an altitude of 80 m. The site was selected as representative of the natural vegetation and regional topography. The climatological average rainfall exhibits a marked seasonal dependence, with a mean monthly maximum of about 350 mm in March, dropping to a mean monthly minimum of around 100 mm in August. This type of forest is estimated to cover 65 to 70 percent of the Amazonian area (Pires 1978). The subsections below describe the measurements made at the site.

a. Routine meteorological measurements

Routine meteorological measurements were provided by two automatic weather stations (Didcot Instruments, Abington, UK) mounted at a height of 45 m on an aluminum scaffolding tower, approximately 10 m above the top of the forest canopy. In these stations, 12 sample measurements (at 5-min intervals) were used to construct the hourly average values of net and solar radiation, air temperature, (aspirated) wet bulb depression and wind direction. Hourly wind speed and rainfall are determined as the integrated counts from a cup anemometer and a tipping bucket raingauge.

The two automatic weather stations (AWS) were run continuously from 1 September 1983 to 30 September 1985, and at least one station was operational for 726 complete days over this period. When both stations were simultaneously available, about 80 percent of the time, the measured variables used in the present analysis were the average from the two stations. When one of the two stations was operational, data were drawn from one station only.

Comparative tests between the two AWSs, and against other independent measurements when these were available, allow estimation of the errors in these routine measurements. Such errors can be systematic, if they are due to logger or sensor calibration, or "pseudorandom," if they are associated with the logging procedure when this involves averaging 12 instantaneous samples of (often rapidly) changing sensor outputs. Systematic errors in the solar and net radiation are estimated at about 5 percent or 5 W m^{-2}, whichever is greater. Temperature is measured only to a systematic accuracy of about 0.5°C, and wet bulb depression to 0.25°C or 10 percent, whichever is greater. Wind direction is prone to systematic error of order 20 deg and wind speed (measured with anemometers with robust, metal caps) is unreliable below 0.5 m s^{-1}, where

the anemometer is prone to stalling, and likely to be subject to systematic errors of at least 10 percent at other times. Systematic errors due to logging or bucket calibration in the tipping bucket raingauge are small, but the measurement shares the susceptibility to systematic "wetting" errors, "splash" errors, and "wind blow" errors common to most raingauges, which are often estimated as on the order of 5 to 10 percent.

Errors in the data generated by the AWS point sample logging procedure most affects the measurements of wind direction, temperature and radiation in rapidly changing daytime conditions. Comparisons between individual hourly measurements of radiation made with the two stations exhibit apparently haphazard differences with a standard deviation on the order of 10 percent. Similar comparisons between temperature measurements and wind direction measurement exhibit a standard deviation up to 0.5°C and 25 degrees respectively. Assuming these fluctuations can be combined statistically as random errors, the random contribution to the total error in the two-station, hourly average values (most commonly used in this analysis) are therefore on the order of 7 percent for radiation, 0.3°C for temperature and wet bulb depression, and 15 degrees for wind direction.

b. *Routine rainfall interception measurements*

Rainfall interception is determined as the difference between the precipitation measurement made above the canopy and the throughfall that reaches the forest floor. The water reaching the ground by flowing down the trunks and stems of the vegetation, the stemflow, was also measured, but was found to be small, on the order of 2 percent of the rainfall. Data were collected from 3 September 1983 to 21 August 1985 and, apart from occasional experimental malfunctions, the interception measurements are available for most of this period. Before July 1984 throughfall was measured with 16 collection gauges randomly relocated at least once each week along a 100 m linear transect; after this time they were randomly relocated at the same frequency on a 100 m × 5 m grid.

Systematic errors in the rainfall measurement above and below the canopy are largely self canceling, but detailed analysis of the sampling errors in the throughfall measurement (see Lloyd and Marques 1988) indicates that these are very considerably greater than those commonly found in similar studies of forests with more uniform structure. This sampling error propagates into the interception loss, which is deduced as a (small) difference between two large terms. Its presence is then exacerbated in percentage terms to such an extent that the resulting individual weekly measurements are difficult to interpret. In consequence, it is only the integrated interception loss over an extended period which provides a valid basis for calibration of the SiB model in the present study. This sampling error is then itself randomly sampled with sufficient frequency that the fractional error in the interception loss assumes acceptable proportions.

In the analysis which follows, the SiB model could be considered to provide a description of the interception process if it yields an estimate of cumulative interception loss which lies in the range $I_j \pm \sigma_j^I$, where the I_j is the cumulative measured interception loss after the jth measurement period, given by

$$I_j = \sum_{i=0}^{i=j} P_i - \sum_{i=0}^{i=j} T_i, \tag{27}$$

and σ_j^I is the estimated error in I_j, given by

$$\sigma_j^I = \left(\sum_{i=0}^{i=j} (\sigma_i^T)^2 \right)^{1/2}. \tag{28}$$

In these expressions P_i, T_i and σ_i^T are the measured precipitation, the measured throughfall and the error in the throughfall measurement for the ith measurement period, respectively. Equation (28) assumes that the sampling error in the throughfall measurement provides the dominant contribution to the total random error. σ_i^T is the standard error calculated from the (initially 16 and later 32) individual throughfall measurements for each measurement period.

c. *Above canopy flux measurements*

The measurements of the above canopy fluxes of momentum, latent heat and sensible heat, which were used to validate/calibrate the aerodynamic and stomatal resistance submodel in SiB, were made with the Mark 1 Hydra instrument. This device provides flux measurements using the eddy correlation technique. It consists of a sensor head (comprising a vertical sonic anemometer, thermocouple thermometer, fast-response infrared humidiometer, and two orthogonally mounted horizontal propellor anemometers), and a microprocessor-based, real-time flux computation unit. The device was installed at a height of 48 m on top of the micrometeorological tower, and operated routinely during September 1983, July and August 1984, and March to August 1985. The data were heavily selected to include only dry canopy conditions in the present analysis. The device is described in more detail elsewhere (see for example Lloyd et al. 1984; Shuttleworth et al. 1984a; Moore 1986).

The systematic and random errors involved in the measured fluxes provided by this still novel device (which may in part respond to the operational environment) can only be estimated by comparison with other instruments. Comparisons between the integrated energy balance provided by the Hydra and the integrated net radiation measurements suggest a systematic error optimistically estimated as 5 percent, and pessimistically estimated as 10 percent, in each of the measured energy fluxes. Systematic error in the momentum

flux measurement is likely to be significantly greater than this, possibly by a factor of 2, because the device uses mechanical sensors to make the horizontal windspeed measurement. In addition, a detailed investigation of the hourly data given by the device suggests that individual hourly heat flux measurements may be prone to apparently haphazard fluctuations which could be at least 10 percent or 10 W m^{-2}, whichever is greater.

Some estimate of the internal consistency of the radiation and heat flux measurements was obtained by summing the hourly net radiation (R_n) and total heat flux ($H + \lambda E$) observations over all the periods where reliable pairs of such data exist. Over the long term the heat storage should be a negligible component of the energy budget. It was found that the time integral of the net radiation measurements over the whole period exceeded the time integral of the heat flux ($H + \lambda E$) measurements by 9 percent. This systematic difference is consistent with the estimates of systematic error given above and is most likely the result of "flux loss" in the eddy correlation device. A similar phenomenon was previously reported in data gathered at this site with this device; see Shuttleworth et al. (1984a). The presence of this imperfect energy balance affected the optimization procedure adopted during calibration; see section 4d.

d. *Leaf stomatal resistance and water potential measurements*

Roberts et al. (1989) made measurements of leaf stomatal conductance on those tree species accessible from the tower throughout the depth of the canopy during three experimental periods, September–October 1983, July–August 1984, and March–April 1985. The measurements were made with a Delta-T transit time porometer (Delta-T Devices, Burwell, Cambridge, UK), with observations concentrated in the upper half of the canopy. These data were analyzed by Roberts et al. (1989) and in the present paper are used to estimate a mean stomatal response to PAR flux and environmental stress (see appendix B). Leaf water potentials were measured on two species, Piptadenia suavolens, (an emergent species projecting above the bulk of the canopy) and Bocoa viridiflora (a subemergent species typical of the bulk of the canopy where most of the shortwave radiation is intercepted) during July and August 1983 and in March 1985. These data were taken using a pressure bomb on successive samples of up to six leaves to yield time series of leaf water potential values. Three days of data for each species were used in the present study, with the mean canopy leaf water potential estimated for each daylight hour by linear interpolation between the available measurements. In all, 16 values of leaf water potential were available for Piptadenia suavolens and 26 values for Bocoa viridiflora. The stomatal resistance data were used for validation but the leaf water potential data were incorporated into the optimization exercise.

4. Model validation and calibration

SiB was designed to be used in general circulation models, and the required meteorological forcing consists of the visible (PAR) and near-infrared direct and diffuse radiation fluxes; the downward longwave radiation flux; temperature, water vapor pressure and wind speed at the reference level; and precipitation (see Table 1a). In this study, the input was provided by the meteorological measurements of solar radiation, temperature, humidity, and precipitation as given by the automatic weather stations. It was therefore necessary to derive the downward longwave radiation, and to partition the measured solar radiation into direct and diffuse components and further partition it into visible and near-infrared portions using empirical relationships; see section 4a.

All the simulations discussed in this paper use the parameters listed in column II of Table 2 and column II of Table 4, except where otherwise specifically stated. The parameters given in Tables 2 and 4 were merged with one of the sets of physiological parameters in Table 3 for a given simulation and are referred to by their column names in that table, viz. literature review, Pearcy, optimized, and Roberts et al.

The prognostic variables used in SiB (see Table 1c) were initialized prior to a simulation run though the model's sensitivity to the initial values of the temperatures T_c, T_{gs}, and T_d and the water stores M_c and M_g is slight; see Sellers and Dorman (1987). All temperatures were initialized to the average measured air temperature, T_r, for the first day in the present case, while the vegetation water stores were initialized to zero. Soil moisture tension was monitored at the site and initial estimates of W_1, W_2 and W_3, the soil moisture contents of the three layers, were obtained from Eq. (22) using these observations in conjunction with the soil parameters given in Table 2. Clearly, such indirect estimation of the soil moisture is prone to error but, in this case, both the measured and calculated soil moisture tension remain low and have little effect on the transpiration flux.

The object of the present study is to validate and where necessary respecify the parameters employed in SiB to describe the TF biome such that the model adequately describes (i) the measured radiation fluxes, (ii) the measured canopy aerodynamic properties, (iii) the integrated interception loss, (iv) the measured latent and sensible heat fluxes within experimental error. The above points are discussed in turn in the next four subsections.

a. *Radiation fluxes*

During model simulations, the spectral and angular properties of the leaves and litter-covered soil surface

were prescribed in SiB following Table 2. Only the total incoming shortwave flux was measured, and the component spectral and angular fluxes had therefore to be estimated using the scheme of Goudriaan (1977), which divides up the total flux on the basis of solar angle and total cloud cover. Solar angle can be calculated astronomically but, in the absence of any other information, the cloud fraction was taken as the monthly climatological average for Manaus given by Ratisbona (1976), irrespective of the time of day or day of the month. Figure 3 shows the typical calculated variation of shortwave albedo given by SiB as a function of solar angle, together with data from Shuttleworth et al. (1984b). The data suggest a mean albedo of about 12%, which agrees with the midday value of 11.7% reported for a Southeast Asian forest by Pinker et al. (1980). The albedo given by the model is high, by 2% or 3%, but nonetheless adequate for GCM applications, both in terms of its magnitude and its dependence on the solar zenith angle. Since there is no allowance for the effect of "clumped" foliage on the interception of shortwave radiation in SiB, the radiative transfer submodel is expected to overestimate the canopy reflectances in both visible and near-infrared wavelength intervals (see Baldocchi et al. 1985).

Figure 3 also shows the calculated effect of different leaf angle distributions on the albedo. These give rise to small changes in the amount of radiation absorbed, but the exact form of the leaf angle distribution is shown to have little impact on the quality of the simulation.

The downward longwave radiative flux was not routinely measured at the site and two techniques were

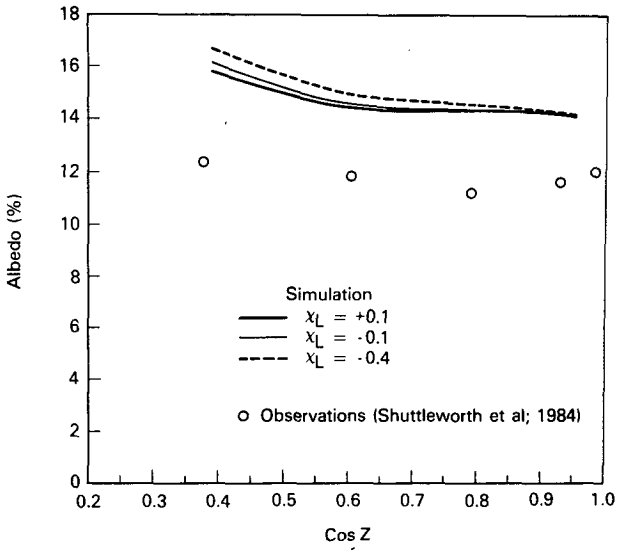

FIG. 3. Measured and calculated variation of albedo with cosine of solar zenith angle (cos Z) for the site during September 1983. The three lines represent different leaf orientations: $\chi_L = 0.1$ is a near random leaf angle distribution, $\chi_L = -0.1$ is a moderately erectophile distribution, $\chi_L = -0.4$ is an extremely erectophile distribution. The observations are from Shuttleworth et al. (1984).

used to estimate it in the simulations presented here. The first, referred to as the empirical method, makes use of an empirical expression given in Monteith (1973), namely,

$$F_{t,d} = \epsilon_a(1 + 0.2C^2)\sigma T_r^4, \qquad (29)$$

where $F_{t,d}$ is downward longwave flux (W m^{-2}), T_r is air temperature at the reference level (K), ϵ_a is apparent emissivity of the air, C is cloud cover fraction, and σ is the Stefan–Boltzmann constant (W m^{-2} K^{-4}), with the apparent emissivity of the air, ϵ_a, given by

$$\epsilon_a = 0.52 + 0.06\sqrt{e_r}, \qquad (30)$$

where e_r is the vapor pressure at reference height (mb).

This simple specification of longwave exchange gives a surprisingly good calculation of net radiation. Figure 4a shows the results of a SiB simulation using all 25 months of the available input data together with the optimized parameter set given in Table 2(II). It is clear that the model produces adequate estimates of net radiation using this method. (Note: in Fig. 4a, as in other figures in this paper, observed and calculated fluxes are compared using a simple "binning" scheme. When a flux measurement was available, the calculated SiB flux value was placed in its appropriate bin and the associated measurement placed in an identically specified bin. At the end of the run, the mean and standard error of the measured values were derived and plotted.) In principle the relationship between observed and calculated net radiation could be sensitive to the physiological parameters used in the simulation, since these can change the surface temperature of the vegetation. Comparisons between simulations with different physiological parameters, however, revealed negligible differences in the radiation simulation.

A second method of estimating downward longwave fluxes, referred to as the "strapped" method, was devised to ensure optimal modeled net radiation flux for simulations investigating energy partition. The calculated net shortwave and the upward longwave flux can be subtracted from the measured net radiation to give an estimate of the net downward longwave flux, thus

$$F_{t,d} = R_n - F_s(1 - \alpha) + F_{t,\uparrow}, \qquad (31)$$

where $F_{t,d}$ is estimated downward longwave flux (W m^{-2}); R_n is measured net radiation flux (W m^{-2}); F_s is measured downward shortwave flux (W m^{-2}), which equals the sum of F_v and F_n; α is estimated surface shortwave albedo; and $F_{t,\uparrow}$ is calculated upward longwave flux (W m^{-2}). The calculation on the right-hand side of Eq. (31) can be made at a particular time step during model operation, and the derived value used as an estimate of the downward longwave flux for the subsequent step. Since downward longwave radiation is a slowly varying quantity, the estimate provided by Eq. (31) provides an acceptable value of net radiation. In practice, using the "strapped" method is equivalent

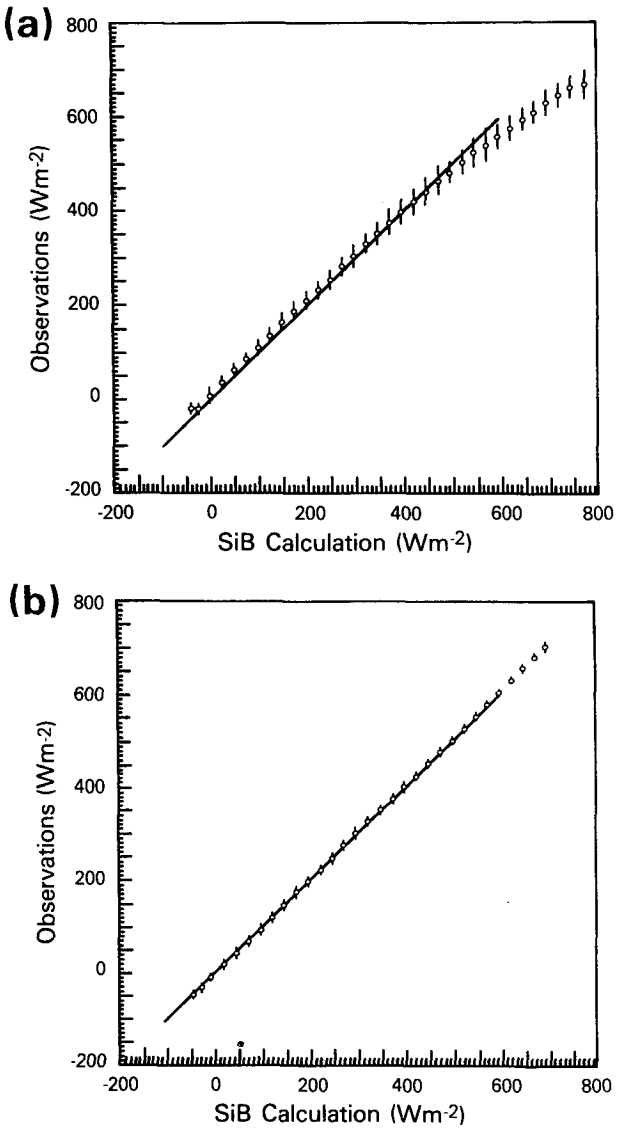

FIG. 4. Comparison of observed and calculated net radiation, R_n, values as obtained using the optimized physiological parameter set applied to 25 months of data. (a) Results obtained using the empirical downward longwave radiation calculation; see (29) in text; (b) results obtained using the "strapped" longwave radiation calculation; see (31) in text. The vertical dashes represent standard errors in the measured values within each bin; see text.

to forcing the observed and modeled net radiation fluxes to agree; see Fig. 4b.

b. *Turbulent transfer*

Two methods for calculating the turbulent transfer properties of the vegetated surface are reviewed in section 2b and appendix A of this paper. Figure 5a compares the calculated and observed values of the friction velocity, u_*, produced using the original (height-invariant foliage density) formulation. The points come from a 25 month simulation run using the aerodynamic properties listed in Table 4, column I, with the optimized physiological parameter set (which ensures that the heat fluxes are approximately correct). Clearly, this formulation yields values of u_* which are too high compared to the data and this suggests that the value of $z_0 = 4.49$ m is too large. Figure 5b shows equivalent results obtained using the aerodynamic description now used by SiB and described in appendix A, which yields a lower value of $z_0 = 2.02$ m. In this case, the observed and calculated u_* values agree fairly well.

Figure 5c also shows results obtained using the new aerodynamic description but in this case with physiological parameters taken from the literature review. The sensible heat fluxes calculated by the model are much lower than observations in this case (see section 4d) and this reduces u_* through increased atmospheric stability. This last result highlights the coupling that can occur between the energy partition and the turbulent transfer properties of vegetated surfaces.

The redefined turbulent transfer scheme better describes the surface aerodynamic properties for this site while also agreeing more closely with the results of Shaw and Pereira (1982); see appendix A. An elevated tropical forest canopy, which reaches its maximum density nearer the tree tops, presents a smoother surface to the airflow than a canopy where the leaf area density is more nearly constant with height. It follows then that tall dense vegetation with elevated crowns may have z_0 values lower than those estimated from the commonly used empirical expression $z_0 \approx 0.13 z_2$; for example, see Monteith (1973). (Note: The original SiB turbulent transfer model gave a value of $z_0 \approx 0.128 z_2$ in this case.) This result is further reinforced by the better match between simulated and measured wind speeds in the upper portion of the forest canopy, see Fig. A3a and A3b.

It should be noted that the three simulations illustrated in Fig. 5a–c all assume a leaf area index of 8. In fact, as discussed later, optimization yielded a mean best-fit leaf area index of 5.01. However, using this value of leaf area index in the SiB momentum transfer submodel produces little change in the aerodynamic parameters (see Table 3, column III), or the value of u_* (see Fig. 5d). The vertical distribution of foliage used in this new model is, therefore, more important than the leaf area index in determining z_0 and d.

c. *Interception loss*

The rainfall reevaporated after interception by the forest is primarily a function of the amount of water that can be stored on the leaves and the aerodynamic properties of the canopy, and has little dependence on physiological parameters (see section 2d). Figure 6 shows the results of four separate 25-month simulations, and compares the model calculated cumulative interception loss with field measurements. All four

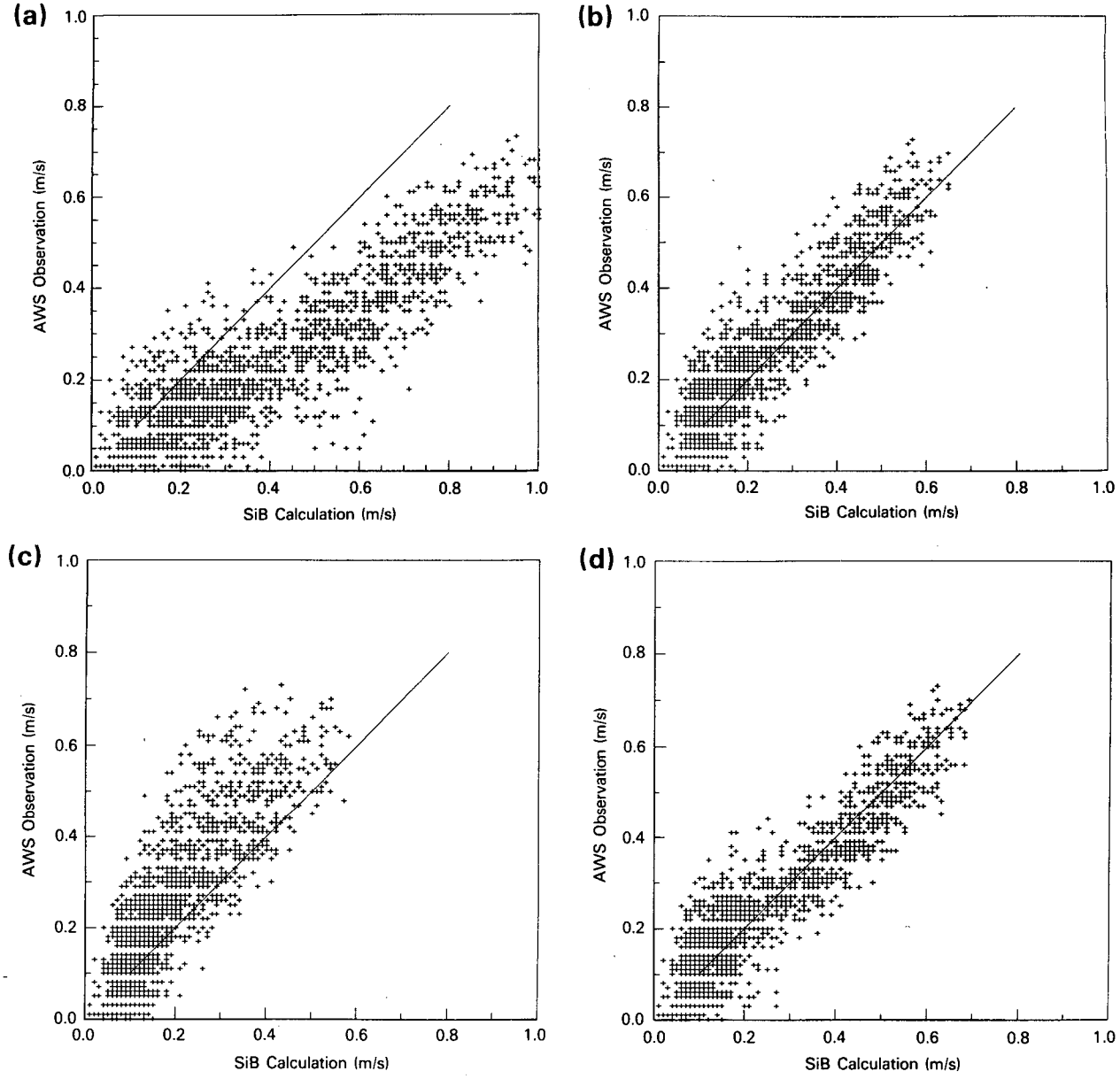

FIG. 5. Comparisons of observed and calculated friction velocity, u_*, values. In all cases, the calculated values were extracted from 25 month simulation runs for those times when matching eddy correlation observations of u_* were available. (a) Calculated values of u_* derived using the original SiB turbulent transfer description which assumed constant foliage density between the canopy base and top; Table 3, column I. The optimized parameter set (Table 4, column III) was used. Canopy leaf area index = 8.0. (b) Calculated values of u_* derived using the new SiB turbulent transfer description which assumes a triangular foliage density distribution, see appendix A and Table 3, column II. The optimized parameter set (Table 4, column III) was used so that the sensible and latent heat fluxes agree fairly well with observations, see section 4d. Canopy leaf area index = 8.0. (c) Same as in (b) except that the literature review parameter set (Table 3, column II; Table 4, column I) was used. This gives rise to much lower estimates of the sensible heat flux and therefore a reduction in the calculated values of u_* through the resulting stable conditions. Canopy leaf area index = 8.0. (d) Same as (b) except that a leaf area index of 5.01 instead of 8.0 was used in the momentum transfer coefficients. In spite of this relatively large change in leaf area index, the calculated u_* values are very similar to those shown in panel (b). See also Table 3, column III; Table 4, column III.

simulations were performed using the optimized physiology data set but the canopy storage was specified differently in each case. These simulations are the four combinations of two leaf area indices and two assumed interrelationships between maximum canopy interception capacity, S_c, and total leaf area index, L_t. The two values of leaf area index, 8.00 and 5.01, correspond to the literature review and optimized parameter sets, respectively. In each case S_c was first set equal to 0.25 mm of water per unit leaf area index (the original SiB

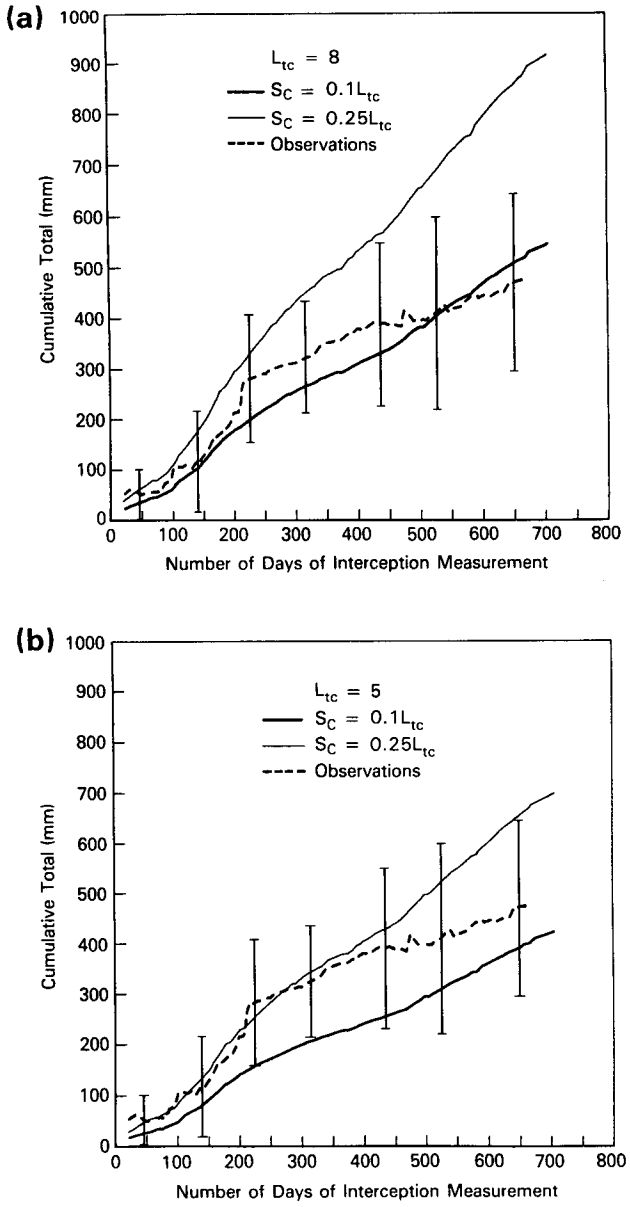

FIG. 6. Plot of cumulative interception loss over the 25-month period. The vertical error bars represent the range of interception loss estimates consistent within one standard error of the observations (see text). The dotted lines represent SiB calculated values for two different values of the total canopy leaf area index, L_{tc}, and two methods of calculating the canopy's maximum interception water storage capacity, S_c. (a) L_{tc} = 8.0, S_c = 0.25L_{tc} mm and S_c = 0.1L_{tc}; (b) L_{tc} = 5.01, S_c = 0.25L_{tc} mm and S_c = 0.1L_{tc} mm.

specification based on observations made in coniferous canopies by Hancock and Crowther 1979) and then set equal to 0.1 mm of water store per unit leaf area index. Figure 6 clearly shows that the second estimate of S_c yields a calculated interception loss in better agreement with observations regardless of the leaf area index used in the simulation. Accordingly, the parameterization used in the SiB model has been altered to use $S_c = 0.1 L_t$ mm for nonconiferous vegetation.

d. *Physiological control of the partition of energy*

There are two ways to obtain the parameters used in SiB to describe a given biome or site. The first is to specify values from the literature or in consultation with individual experts, a method which proved adequate for arable crop and coniferous forest sites (Sellers and Dorman 1987), and which is probably also adequate in specifying the morphological parameters given in Table 2. If no relevant and reliable micrometeorological measurements exist, this method remains the only option. The second method, explored for the first time in this paper, is to use experimental data comprising simultaneous near-surface measurements of meteorological variables and surface fluxes, and then to optimize those parameters for which most uncertainty exists. This last technique involves operating SiB inside an iterative loop driven by a least-squares reduction program. The procedure is as follows:

(i) The input parameters to be optimized are initially set to plausible values, generally those given by the literature review (Table 4, column 1).

(ii) A SiB simulation is made using the near-surface meteorological data as forcing variables, to calculate heat and radiation fluxes, and various physiological variables; canopy resistance, leaf water potential, etc.

(iii) The quality of the agreement between the calculated and the observed fluxes is assessed by taking the difference between the calculated and the observed evaporative fraction, thus

$$F_i = \left[\left(\frac{\lambda E_i}{\lambda E_i + H_i}\right)_C - \left(\frac{\lambda E_i}{\lambda E_i + H_i}\right)_O\right] |\lambda E_i|_O, \quad (32)$$

where F_i is the deviation calculated for time step i, and λE_i, H_i are the latent, sensible heat fluxes for time step i (W m^{-2}). The subscripts "C", "O" refer to calculated and observed values respectively. This deviation is weighted by the absolute value of the observed latent heat flux, $|\lambda E_i|_O$, so as to assign greater importance to higher (daytime) fluxes. The use of the evaporative fraction as a discriminator in the optimization procedure ensures the stability of the optimization in the presence of an imperfect energy balance in the experimental data, see section 3c. In (32), we assume that the ratio of the observed heat fluxes is correct, even if the absolute values are in some doubt.

The mean deviation error, $\bar{F}$, is defined by

$$\bar{F} = \left(\frac{1}{N}\sum_{i=1}^{N} F_i^2\right)^{1/2}, \quad (33)$$

where N is the number of calculated, observed flux pairs, and can be considered broadly equivalent to the mean deviation in the calculated latent heat flux, in W m^{-2}.

(iv) The set of deviations, F_i, is used in an IBM least-squares minimization program, ZXSSQ (see IMSL 1984), to numerically determine the partial derivatives of F_i with respect to the optimized parameters. The parameters are then altered to reduce F_i. When F_i cannot be reduced further or the partial derivatives of F_i fall below a specified value, optimization terminates to yield the physiological parameters that give the best fit.

The primary aim of this study was to obtain the best possible *single* set of parameters for the site, assuming constant leaf greenness and leaf area index. Accordingly, five 2 week periods were chosen when the heat flux data were available and instrument reliability was reasonably high. The timing of these periods and the number of flux measurements available within each are shown in Table 5a. A total of 947 flux measurements were available from these five periods from which a single ("best-fit") set of physiological parameters were obtained by the iterative process described above. Typically, 300 iterations were required to achieve convergence.

A separate optimization was made using data collected over a 20-day period for which leaf water potential measurements were also available (see Table 5b). In this case the optimization procedure was modified so that it minimized the difference between observed and calculated leaf water potentials in addition to, or instead of, the heat fluxes. A weighting procedure was used such that the contribution to the sum of squares given by flux deviations and leaf water potential deviations were roughly equivalent. This study is discussed first.

Table 6 shows values of the physiological parameters for several different optimizations carried out on the period specified in Table 5b for which leaf water potential data are also available. Also shown, for comparison, are results obtained with parameters specified by the literature review (column I). The sum of the deviations in flux and leaf water potential are given as appropriate. Column II in Table 6 shows the results obtained when only the flux deviations are used in the optimization: the sum of squares of the flux deviations is 28 077, and the value of ψ_{c2} is comparatively low (-564.8). Columns III, IV and V of the Table 6 compare the results obtained by including different sets of leaf water potential observations in the optimization: Column III includes data for Piptadenia suavolens only, column IV data for Bocoa viridiflora only, and column V data for both species. Figure 7 illustrates the comparison between model calculated and observed leaf water potential in the last case. Three observations can be made on these results. First, the two tree species favor different minimum values of ψ_l, corresponding to their respective positions in the canopy: the emergent Piptadenia suavolens, which is exposed to more radiation and a higher evaporative demand, might be expected to support a lower minimum leaf water potential than the subemergent Bocoa viridiflora. Second, it was possible to provide a good fit to the *flux* data while simultaneously optimizing on the combined set of leaf water potential data (column V). The sum of squares in this case was 28 456, only slightly larger than the optimization on flux alone (column II). This suggests that the best average physiological data set is intermediate to two tree species studied, and is probably biased towards the subemergent Bocoa viridiflora which may be more representative of the canopy as a whole. Last, the results indicate that leaf water potential is closely linked to the canopy resistance and transpiration rate and the values of h_5 and R in column V suggest that both $f(\delta e)$ and $f(\psi_l)$ play significant roles in limiting transpiration.

The importance of these two controls is explored further in columns VI, VII and VIII of Table 6. These show the results when jointly optimizing both on the observed fluxes and the leaf water potential data (for both tree species), as before, but with $f(\psi_l)$ set to unity in column VI, $f(\delta e)$ set to unity in column VII, and both $f(\delta e)$ and $f(\psi_l)$ set to unity in column VIII. These

TABLE 5. Characteristics of the five measurement periods used in (a) the heat flux optimization procedure and (b) the single extended measurement period used in the combined leaf water potential and heat flux optimization procedure. Forty-two estimates of mean leaf water potential (from two canopy species) were available for this period.

Period	Start date (yr/mo/day/h)	End date (yr/mo/day/h)	Duration (h)	Number of flux measurements (dry canopy only)	Mean daily precipitation (mm)	Mean Bowen ratio $\int Hdt/\int \lambda Edt$ (dry canopy only)
(a) Heat flux optimization procedure						
1	83/09/04/11	83/09/19/02	352	200	7.33	0.35
2	84/08/09/07	84/08/23/01	331	200	5.82	0.28
3	85/04/11/09	85/04/26/08	360	170	8.78	0.23
4	85/06/11/09	85/06/26/08	360	177	6.17	0.16
5	85/09/12/10	85/09/26/06	333	200	3.44	0.37
(b) Combined leaf water potential and heat flux optimization procedure						
6	84/07/31/00	84/08/19/23	480	184	5.80	0.25

TABLE 6. Results of optimizing physiological parameters using period 6 described in Table 5b. Different combinations of leaf water potential data sets were used to produce the results shown in columns II through V. Columns VI through VIII explore the roles of the leaf water potential and vapor pressure deficit stomatal responses in controlling transpiration.

Parameter	I	II	III	IV	V	VI	VII	VIII
a	4765.0	2873.7	2513.7	4590.9	2439.1	2929.2	2899.6	3787.7
b	16.5	−0.036	0.039	−0.069	−0.004	0.021	0.026	−0.084
c	33.0	193.4	161.6	131.1	163.7	204.0	165.7	231.4
h_5	0.0222	0.0221	0.0179	0.0234	0.0248	0.0254	0.0216	0.0216
ψ_{c_1}	−200.0	−46.0	−26.6	−7.57	−15.8	−50.8	−75.4	−50.8
ψ_{c_2}	−500.0	−564.8	−966.2	−1417.0	−1325.8	−424.2	−475.6	−424.2
R	20 000.	24 020.	2966.	4989.	3862.	3699.	4052.	4620.
L_{lc}	8.0	6.47	7.12	7.33	6.31	5.70	6.13	4.81
N_c	0.98	0.947	0.949	0.948	0.949	0.949	0.949	0.747
Σ deviation (Flux)	326 170	28 077	44 931	28 912	28 456	36 864	41 012	49 932
Σ deviation (ψ_l)	—	—	29 289	46 472	188 850	184 680	213 280	243 540

I. Initial value parameter set, same as literature review parameter set.
II. Optimization carried out using the flux data only.
III. Optimization carried out using flux data and P. suavolens leaf water potential (ψ_l) data.
IV. Optimization carried out using flux data and B. viridiflora ψ_l data.
V. Optimization carried out using flux data and both P. suavolens and B. viridiflora ψ_l data (see also Fig. 7).
VI. Same as V, except that leaf water potential effect on stomatal resistance has been decoupled; $f(\psi_l) = 1$.
VII. Same as V, except that vapor pressure deficit effect on stomatal resistance has been decoupled, $f(\delta e) = 1$.
VIII. Same as V except that both leaf water potential and vapor pressure deficit effects on stomatal resistance have been decoupled, $f(\psi_l)$; $f(\delta e) = 1$.

optimizations therefore examine the effect of decoupling the $f(\psi_l)$ and $f(\delta e)$ controls from canopy resistance. In all cases, the sum of the mean flux deviation is significantly larger than the result shown in column V, which suggests that *both* of these factors play significant roles in controlling stomatal function.

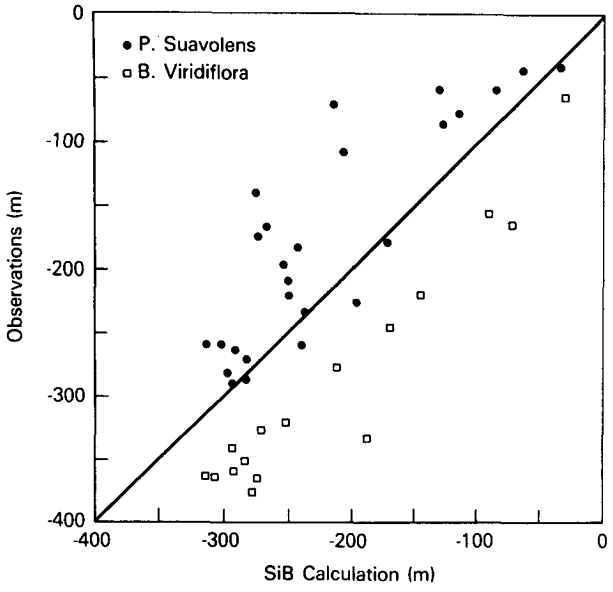

FIG. 7. Comparison of observed (from data of Roberts et al. 1989) and simulated (see Table 6, column V and text) canopy leaf water potential, ψ_l, values. Note that observations are for two species; P. suavolens and B. viridiflora, and that these two species have substantially different ψ_l responses to meteorological conditions, presumably adaptations to their different positions in the canopy. The simulation produced physiological parameters that attempt to provide the best average fit to both sets of data, as can be seen from the way the 1:1 line in the figure almost separates the data for the two species.

The catenary model used in SiB is simplistic (see Sellers et al. 1986 and section 2d) in that it does not acknowledge hormonal control or plant storage. (It is entirely possible that the bulk of a day's transpiration may be extracted from plant tissue which is recharged at other times of day.) At the same time, inspection of time series of simulated and observed leaf water potential does not reveal any significant phase difference. The assumed link between $f(\psi_l)$, ψ_l and transpiration seem to produce realistic results even if the paradigm is not entirely correct.

The physiological parameters listed in column V of Table 6 were used as the initial values for the more extensive parameter optimization performed using the five 2-week periods listed in Table 5a. No leaf water potential data are available in this case, and optimization is merely against deviations in measured flux. The resulting optimized parameters given in Table 3, column III are the preferred values that now provide the calibration of the TF biome in the SiB model.

Figures 8, 9 and 10 compare simulations carried out using the literature review, Pearcy and optimized parameter sets, respectively. Diagrams (a) and (b) in each figure compare the observed and calculated latent and sensible heat fluxes respectively. The strapped radiation calculation was used in each case, thereby ensuring a good simulation of net radiation. It is clear from Fig. 8 that the literature review parameters provide a poor comparison with observations because canopy con-

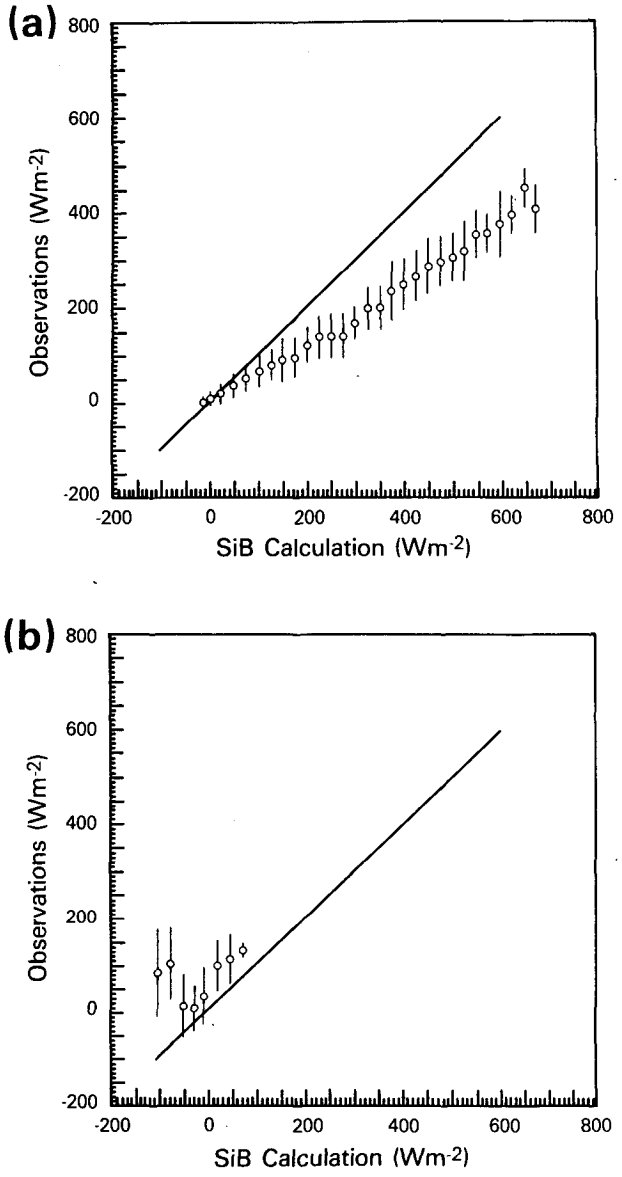

FIG. 8. Comparison of observed and calculated values of (a) latent heat flux, λE, and (b) sensible heat flux, H, with calculated values obtained from the literature review parameter set. The "strapped" longwave radiation scheme was used.

ductance is overestimated (see Fig. 2). The Pearcy parameters give a better comparison with the data (see Fig. 9) although the calculated canopy conductance is still too high and the diurnal trend inaccurate (as shown by the curvature in the sensible heat flux comparison). Not surprisingly, Fig. 10 shows the optimized parameters calculate fluxes which compare well with observations, with some overestimation of the fluxes at higher values. This is merely because the modeled heat fluxes are constrained by measured net radiation which, on average, exceeds the sum of the observed heat fluxes by 9 percent; see section 3c. The mean residual deviation produced by each set of parameters are given in Table 7.

As previously mentioned, the surface resistance, $\bar{r}_c$, is dominant in determining the energy partition of tall, dry vegetation. Figure 11a shows calculated values of $1/\bar{r}_c$ as a function of above canopy PAR flux density using the optimized physiological parameters (Table 4, column III) over the 25-month period for which AWS data were available. In this diagram the upper limit of the data points corresponds to the maximum value of canopy conductance for a given PAR flux density, which is only achieved when there is no temperature, vapor pressure deficit or leaf water potential stress acting in the canopy. These stresses commonly reduce the canopy conductance by a factor of 2 to 3. Shuttleworth et al. (1984a) report a median value of surface resistance for this forest canopy around 100 s m^{-1} during the middle of the day, a value consistent with these calculations. Figure 11b shows equivalent results obtained with the literature review parameter set, and show, in this case, canopy conductances consistently three or four times higher than those in 11a.

e. Discussion

The values of the optimized parameters shown in Table 4 can be assessed in terms of their physical and physiological credibility.

The optimized values of leaf area index and canopy greenness, 5.01 and 0.905 respectively, appear reasonable and fall within the range of values reported in the literature. Medina and Klinge (1983), Mooney et al. (1984) and Schulze (1982) report TF leaf area indices ranging from 5 to 12, with a mean of 7, and no significant dead foliage in the canopy. There are two reasons why the optimized value of L_{tc} might be biased towards the lower end of this range. First, the periods used in the optimization are themselves biased towards the dry season, since periods were selected to include a significant proportion of dry canopy conditions. Roberts and Shuttleworth (personal communication) noted a considerable number of dead leaves in the canopy and on the ground in September, with new leaves

TABLE 7. Mean residual deviation, in W m^{-2}, generated by each set of parameters for each of the periods in Table 5. Also shown is the mean error deviation over all periods. The deviation is defined by Eq. (33) in the text.

Period	Literature review	Pearcy	Optimized	Roberts et al.
1	43.8	36.4	14.3	16.9
2	44.6	30.7	13.1	12.9
3	37.8	27.8	12.9	10.8
4	27.0	13.6	12.5	10.9
5	56.1	42.8	15.0	18.9
6	42.1	26.9	13.7	12.7
Mean	41.9	29.7	13.6	13.9

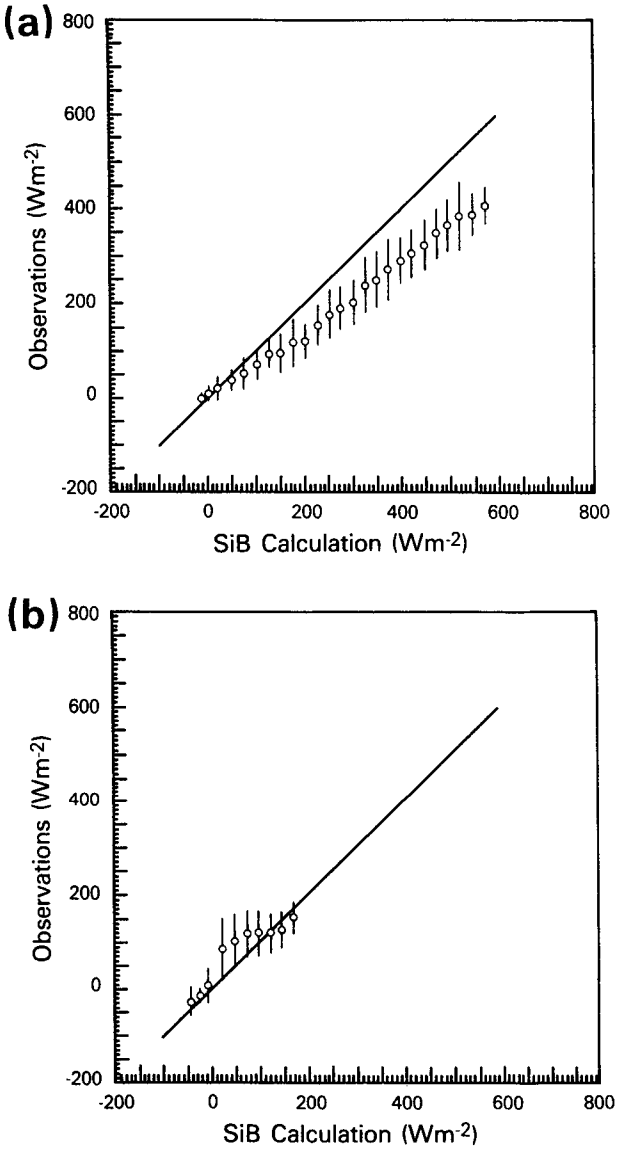

FIG. 9. Comparison of observed and calculated values of (a) latent heat flux, λE, and (b) sensible heat flux, H, with calculated values obtained from the Pearcy parameter set. The "strapped" longwave radiation scheme was used.

emerging in October. The second possible cause is the hypothetical "clumping" of the canopy foliage mentioned in section 4a. As the leaves in a canopy become increasingly clumped, the average canopy conductance drops due to increased mutual shading of leaves. Since SiB does not explicitly acknowledge this feature, it could easily misinterpret the origin of this reduced conductance as a reduced leaf area index during optimization.

The physiological constants derived from the optimization compare well with those derived from analysis of the data of Pearcy (1987) and Roberts et al. (1989; see appendix B), but poorly with the mean values extracted from the literature (see Table 4). The light response parameters for the optimized, Pearcy and Roberts et al. parameter sets in fact give rise to very similar stomatal resistance/conductance trends; see Fig. 2.

The parameters describing the operation of leaf water potential in SiB were obtained by optimizing against the observation of Roberts et al. (1989), as described in a previous section. The value of $\psi_{c_1} = -15.$ m implies that the leaf water potential effect operates even at very low transpiration rates. The leaf water potential "shut-down" value of $\psi_{c_2} = -1553.$ m appears, to be

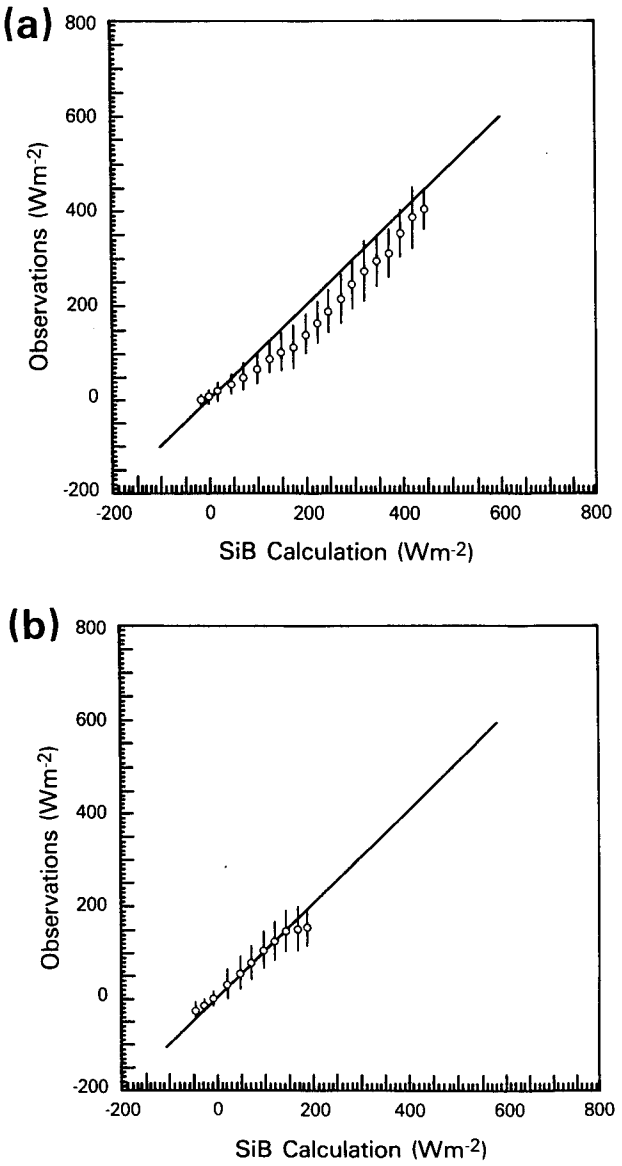

FIG. 10. Comparison of observed and calculated values of (a) latent heat flux, λE, and (b) sensible heat flux, H, with calculated values obtained from the optimized parameter set. The "strapped" longwave radiation scheme was used.

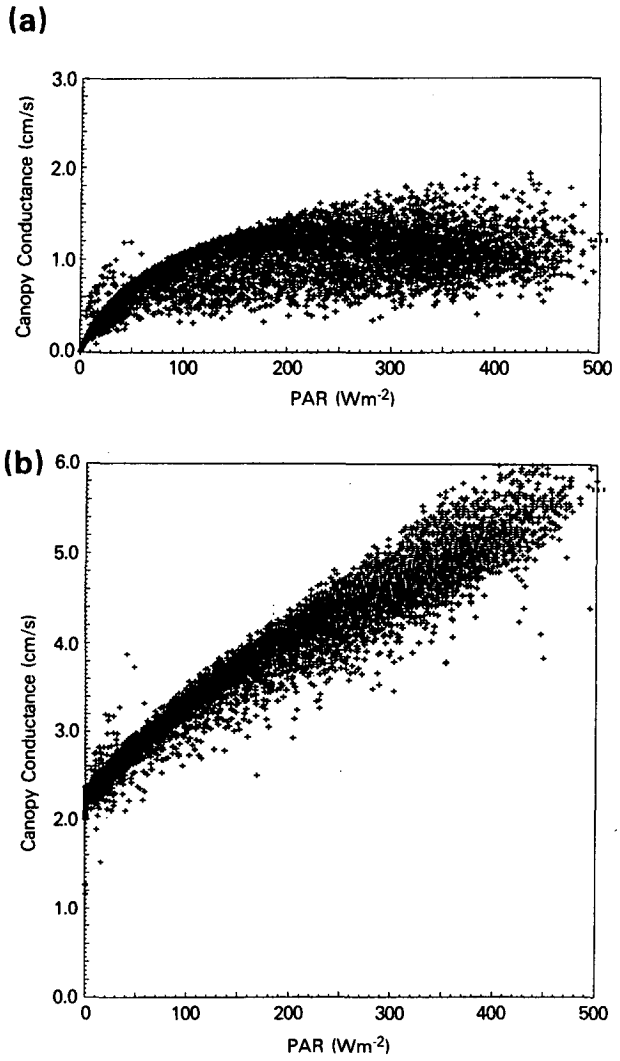

FIG. 11. Calculated values of the canopy conductance, $(1/\bar{r}_c)$, computed using (a) the optimized parameters and (b) the literature review parameters, plotted against PAR flux density. A conductance value of 1 cm s^{-1} is equivalent to a resistance of 100 s m^{-1}. The points correspond to $1/\bar{r}_c$ values obtained for each hour when flux data were available. Total leaf area index, L_{tc}, is 5.01.

too low, if anything, although Roberts et al. (1989) refer to observations of $\psi_l \approx -450$ m for the transpiring leaves of a tropical tree species. It will be remembered that the analysis indicated that $f(\delta e)$ and $f(\psi_l)$ *both* played roles in limiting the canopy conductance. For reasons previously stated, however, it is difficult to separately identify the effects of $f(\delta e)$ and $f(\psi_l)$. Pearcy (1987) published data that indicate a mean value of $h_5 = 0.0226$ for two Australian TF canopy species, which compares well with our optimized estimate of 0.0273. The data of Roberts et al. (1989; analyzed in appendix B) yield a combined stress term $[f(\delta e)f(\psi_l)]$ which was compared with equivalent estimates in a SiB simulation using optimized parameters. In both cases, the apparent slope of $[f(\delta e)f(\psi_l)]$ against δe, referred to here as b_s or b_R [for SiB or Roberts et al. (1989) data, respectively], was determined by linear regression and the results grouped according to the incoming shortwave radiation; see Table B.3. The mean value of b_s for SiB is 0.032, which can be favorably compared with the mean values from the Roberts et al. (1989) data, b_R, of 0.035, 0.040 and 0.042 obtained for P. suavolens, B. viridiflora, and the composite of these two with two additional species, respectively; see appendix B. The stress terms obtained by optimizing the physiological parameters in SiB therefore compare well with observations conducted on individual leaves in situ, which suggests that the values of the parameters governing stress and the stress term formulations themselves are adequate.

The calculated *live* root length per unit area of 5122.3 mm^{-2} may be compared to the equivalent measurement of *total* root length reported by Jordan and Escalante (1980) of 20 000 m m^{-2}. In fact, the optimization procedure merely selects a live root length consistent with the total soil-plant resistance term necessary to provide adequate simulation of observed leaf water potential. The actual value of live root length is therefore entirely dependent on the value *assumed* for other factors in the combined term $(\overline{r_{soil}} + \overline{r_{plant}})$, and little is gained from such comparison.

Perhaps the most interesting result of the optimization is the indicated role of the $f(\delta e)$ and $f(\psi_l)$ stress functions. In particular, it seems that the vegetations response to vapor pressure deficit is strong in this biome. This presumably protects the leaves from desiccation since the high evaporative demand might be difficult to meet along the stem-leaf transfer pathway, even when moisture is freely available in the soil. A vapor pressure deficit of about 20 mb is predicted to approximately double the canopy resistance. Assuming the canopy radiation model is adequate (use of the strapped longwave calculation method in any case assures good estimation of available energy) and that the aerodynamic resistance calculations can provide reasonable values of r_a and $\overline{r_b}$ (see section 4b), the process of parameter optimization with the SiB model clearly can yield reasonable *average* values of leaf area index, canopy greenness and certain critical physiological parameters. These optimized values provide encouraging evidence of the realism of SiB. With an optimization process operating on such a large number of free parameters, it is fairly easy to obtain good agreement between calculated and observed fluxes but an unrealistic model is much less likely to prefer credible physiological and physical parameters. In this case optimization yields parameter values that correspond reasonably well with observation. To this degree, SiB must be biophysically realistic.

Figures 12 and 13 compare three typical days of SiB simulation using the literature review and optimized parameter sets. In both cases, the strapped radiation

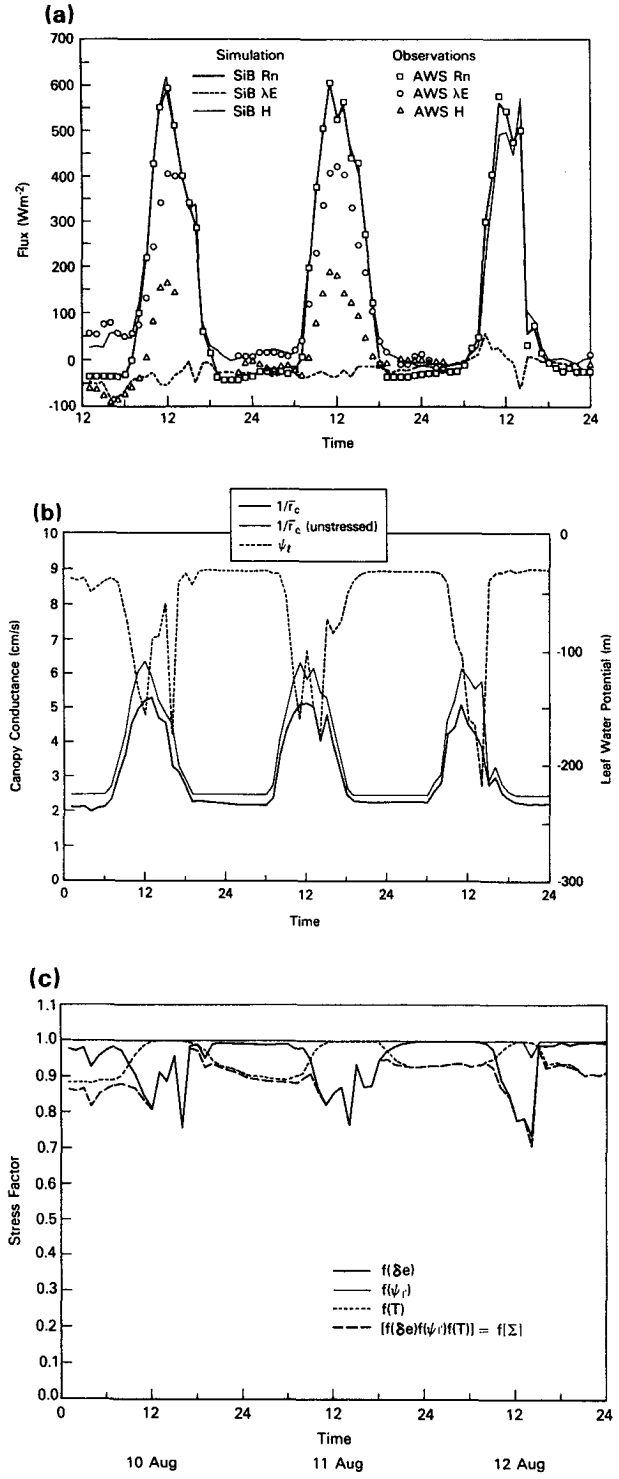

FIG. 12. Results of three days of SiB simulation using the literature review parameter set compared to observations. (a) Time-series of observed and calculated net radiation, latent heat flux and sensible heat flux. The "strapped" longwave radiation scheme was used. (b) Time-series of canopy leaf water potential, ψ_l, unstressed canopy conductance, $(1/\bar{r}_c)_*$, and canopy conductance, $(1/\bar{r}_c)$. (c) Time series of the calculated stress factors $f(T)$, $f(\delta e)$ and $f(\psi_l)$ and their multiple, $f(\Sigma)$.

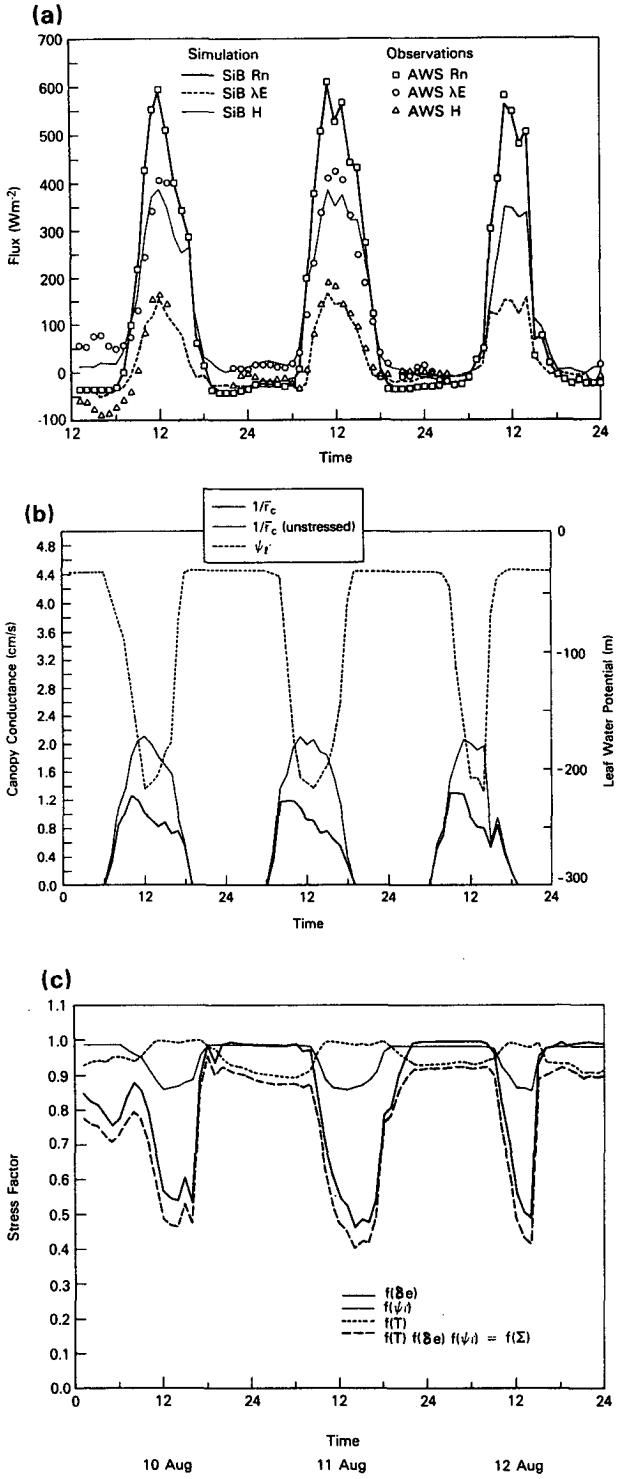

FIG. 13. Results of three days of SiB simulation using the optimized parameter set compared to observations. (a) Time-series of observed and calculated net radiation, latent heat flux and sensible heat flux. The "strapped" longwave radiation scheme was used. (b) Time-series of canopy leaf water potential, ψ_l, unstressed canopy conductance, $(1/\bar{r}_c)_*$, and canopy conductance, $(1/\bar{r}_c)$. (c) Time-series of the calculated stress factors $f(T)$, $f(\delta e)$ and $f(\psi_l)$ and their multiple, $f(\Sigma)$.

procedure was used to force agreement between the calculated and observed radiation. The literature review simulation yields a Bowen ratio close to zero: practically all the available energy is used for evapotranspiration; see Fig. 12a. The canopy conductance varies from a minimum of 2 cm s^{-1} to about 5 cm s^{-1} at midday (see Fig. 12b), with the stress terms giving about 20 percent reduction in the maximum conductance in the afternoon, mainly due to the effect of the vapor pressure deficit. The calculated canopy conductance is more or less symmetrical around midday; see Fig. 12c. The simulation given with the optimized parameters, which is illustrated in Fig. 13, exhibits very different behavior. Latent heat flux now accounts for about 75 percent of the net radiation during the daylight hours; see Fig. 13a. The diurnal course of the calculated canopy conductance, shown in Fig. 13b, is more plausible and interesting. The minimum conductance is low, about one-tenth of the literature review value, which effectively shuts off transpiration at night. During the daylight hours, the *unstressed* value of canopy conductance follows the diurnal course of the shortwave radiation flux and is roughly symmetric about local midday but the actual value is about half the unstressed value and is asymmetric. The three curves shown in Fig. 13b are typical: during the morning, canopy conductance remains unstressed until about 0800. Thereafter, vapor pressure deficit and leaf water potential progressively reduce canopy conductance until the peak value of the vapor pressure deficit, δe, is reached at around 1500. Since the daily pattern in δe is not symmetric about midday, the net effect is a near-linear decline in canopy conductance over the rest of the day. Generally, the actual value of canopy conductance is about half the unstressed value during the early afternoon. This simulated magnitude and asymmetric pattern compares well with the separate analyses of Shuttleworth et al. (1984a) and the data of Roberts et al. (1989). The former shows similarity in both magnitude and trend, while the stomatal resistance data of Roberts et al. (1989) exhibits a near linear decline in leaf stomatal conductance during the late morning and early afternoon. Verma et al. (1986) analyzed a similar set of flux data and produced composite time-series of canopy conductance for a deciduous forest in Tennessee. These results, summarized in Fig. 7 of Verma et al. (1986), bear a remarkably close resemblance to the time-series shown in Fig. 13c of this paper, both in terms of magnitude ($\overline{r_c} \sim 100$ s m^{-1}) and trend (viz. a near linear decline in $1/\overline{r_c}$ over the day).

The main objective of the study described in this paper was to assess the validity of different techniques for calibrating SiB and to obtain a single set of representative parameters. In this study, the tropical forest morphology and physiology was therefore assumed to be invariant on the annual time scale. It is possible to obtain some indication of the verity of this last assumption by plotting the monthly average ratio of the observed and calculated latent heat flux over the annual cycle.

In practice, it is necessary to adjust this ratio to allow for the systematic difference in the measured energy balance between incoming net radiation and the outgoing sensible and latent heat fluxes; see section 3c. To do this, an adjusted heat flux ratio, R_E, was defined as follows:

$$R_E = \sum_{i=1}^{M} \left[\frac{(\lambda E_i + H_i)_C}{(\lambda E_i + H_i)_O} \frac{(\lambda E_i)_O}{(\lambda E_i)_C} \right], \qquad (34)$$

where R_E is the adjusted ratio of observed to calculated (SiB) latent heat fluxes, λE_i, H_i are latent, sensible heat fluxes, respectively, for ith time period in a month (W m^{-2}), C, O are subscripts for calculated (SiB) and observed heat fluxes, and M is the number of reliable flux (H and λE) measurements under dry canopy conditions during a given month.

When R_E is greater or less than unity, the transpiration rate exceeds or drops below the rate calculated for the time-mean canopy condition as specified by the optimized parameter set; see Table 3, column III. Even though coverage of the annual cycle is incomplete, the results of this procedure indicate that there are distinct and statistically significant changes in the energy partition of the forest canopy as a function of time (see Fig. 14a), and these appear to follow an annual cycle (see Fig. 14b). The direct effects of seasonal changes in meteorological and soil moisture conditions on the evapotranspiration rate are already accounted for in the energy balance calculations. The temporal variation in the calculated to observed ratio of evapotranspiration must therefore be due to seasonal variations in the vegetation's physiological characteristics that are not adequately represented by the time-invariant set of physiological parameters. In GCM applications, it is clearly desirable that such variations should be both observed and modeled on regional and global scales. This issue can be addressed using satellite data, and will form the substance of a future paper.

5. Summary

Micrometeorological and heat flux measurements obtained above an Amazonian tropical forest (TF) site were used to validate and calibrate the simple biosphere model (SiB) of Sellers et al. (1986). Comparison between model calculations and observations indicated that, after some modification of the turbulent transfer submodel (appendix A), the momentum flux and radiative transfer components of SiB and the relevant TF parameters, provided adequate descriptions of the turbulent transfer and energy absorption characteristics at this forest site. When the calculated energy partition was compared to observations, it was found that the physiological parameter set obtained from a brief review of the literature (appendix B) consistently overestimated the latent heat flux and canopy conductance.

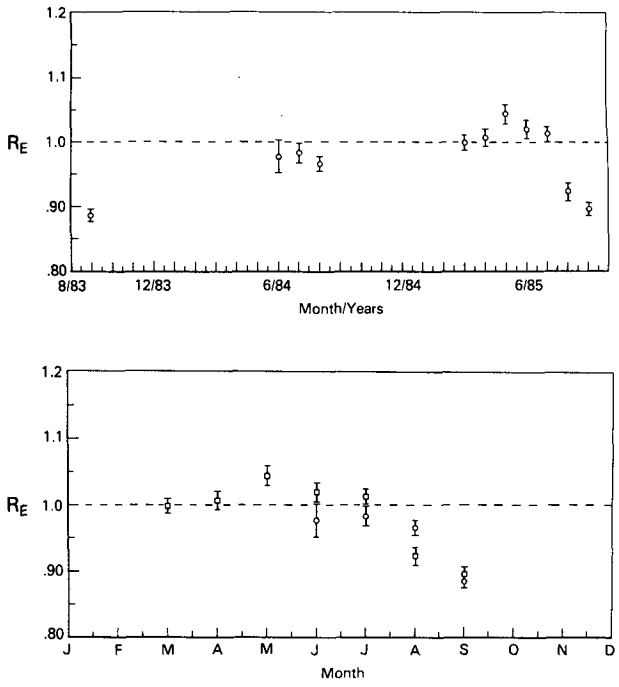

FIG. 14. (a) Variation of the adjusted heat flux ratio of observed and calculated latent heat fluxes, R_E, over the whole experimental period, 1983–85. Only dry canopy fluxes were used in this analysis and the calculated fluxes were obtained using the optimized parameter set. The points marked in the figure are taken from different periods during the 25 months with associated standard errors shown as vertical bars. (b) Composite of the results shown in panel (a) onto a single annual cycle. Note drop in R_E in August–September, repeated from year to year.

An optimization procedure was used to define a set of physiological parameters that gave the best fit between the calculated and observed energy partition for a large number of measurements (947) made over the two-year field campaign. The physiological parameter set so derived gave lower canopy conductance values than those suggested by the literature review and suggested that the stomatal response to vapor-pressure deficit and leaf water potential play significant roles in determining the diurnal course of transpiration from the forest. The derived parameter set corresponded well with leaf conductance measurements obtained locally by Roberts et al. (1989) and equivalent data for an Australian TF site responded by Pearcy (1987).

The optimization procedure described in the text yields estimates of parameters and process rates that are representative of a relatively large area, on the order of 10^4 to 10^6 m^2, rather than of individual leaves or plants. It can be argued that these area-averaged parameters are of more practical use to regional or global scale modelers than species-specific data sets.

Finally, the predicted partitioning of energy by the optimized parameter set was compared to the observed values for different times of the year. It is clear from this that there are distinct seasonal variations in the biophysical properties of the forest canopy and that the assumption of time-invariant parameters is not necessarily realistic. The extent of these variations, their probable causes and the means of monitoring them will be addressed in a future paper.

Acknowledgments. The data presented here were collected in the course of a two-year Anglo-Brazilian study of Amazonian Micrometeorology and represent a very considerable experimental effort. The authors would particularly like to thank John Gash, Chris Moore and Colin Lloyd, from the Institute of Hydrology, and many Brazilian collaborators, notably Luis Molion, Carlos Nobre, Leo de Sa, Ari Marques, Gilberto Fisch, Osvaldo Cabral, Maria Ribeiro, Januario Mauro and Arthemio Fattori. Financial support during data collection was provided by UK Natural Environment Research Council, the Brazilian Conselho Nacional de Desenvolvimento Cientifico and Technologico (CNPq), and the British Council. Dr. Robert Pearcy of Department of Botany, University of California at Davis is warmly thanked for many discussions and the provision of stomatal resistance data for tropical species, and Dr. D. E. Strebel is likewise thanked for providing the dead leaf optical properties.

One of the authors (WJS) is grateful to Professor J. Shukla for the invitation and financial support to visit the University of Maryland, Center for Ocean–Land–Atmosphere Interactions (COLA), which stimulated the work for this paper. He is also grateful to Dr. V. Salomonson, Dr. R. Gurney and other members of the Laboratory for Terrestrial Physics at NASA for their hospitality during this visit.

Piers Sellers and Jeff Dorman were supported by NASA Grant NAG-5-492 throughout this work with additional support from NASA Goddard Space Flight Center arranged by Dr. Baker. Ms. Joyce Tippett edited and typed many different versions of this paper.

APPENDIX A

Modification of the Turbulent Transfer Model of SiB to Accommodate the Variation of Canopy Density with Height

The original version of SiB described in Sellers et al. (1986) considered the canopy as a "constant density block of porous material" extending from height z_1 to z_2, see Fig. A.3a. While this description appeared to yield acceptable values for a variety of vegetation types (see Sellers and Dorman 1987), it gave rise to an excessively high value of u_* for the case of the tropical forest (see Fig. 5a). While realizing that the SiB turbulent transfer model must necessarily be a gross simplification of the real physical processes controlling turbulent transfer within and above vegetated surfaces, it was believed that some simple modification could be made to improve its performance.

Shaw and Pereira (1982) made use of a second-order turbulent transfer description to investigate the relationship between canopy structure and the bulk parameters of surface roughness length, z_0, and zero plane displacement, d. Their results showed a strong dependence of both of these quantities on the vertical distribution of foliage density within the canopy: essentially, canopies with foliage concentrated near their bases were predicted to be rougher (i.e., higher z_0 values, lower d values) than canopies having the same amount of foliage concentrated near the top of the vegetation. The original version of SiB could not take this significant effect into account. Therefore, it was decided that the most appropriate course of action would be to:

(i) Modify the aerodynamic description within the canopy to take account of the nonuniformity of the foliage density profiles and,

(ii) Modify the links between the within-canopy profiles to the above canopy transition layer profiles in such a way as to yield results as close as possible to those generated by Shaw and Pereira (1982).

Each of these tasks is discussed in turn below.

a. Within-canopy profiles of wind speed and momentum transfer coefficient

The equations assumed to govern the absorption of momentum by the canopy in SiB, are

$$\tau = \rho K_m \frac{\partial u}{\partial z} \tag{A.1}$$

$$\frac{\partial \tau}{\partial z} = \rho \frac{C_d \overline{L_d} u^2}{p_s} \tag{A.2}$$

$$K_m = \sigma u, \tag{A.3}$$

where τ is shear stress (kg m^{-1} s^{-2}), ρ is air density (kg m^{-3}), u is wind speed (m s^{-1}), z is height (m), C_d is phyto-element drag coefficient, p_s is shelter factor, $\overline{L_d}$ is area-averaged leaf area density (m^2 m^{-3}), and σ is a constant to be determined by calculation. The parameters C_d and p_s are defined as in Sellers and Dorman (1987).

Previously, $\overline{L_d}$ was held constant with height between z_1 and z_2. To describe a canopy with a triangular leaf area density distribution, we introduce the following equations:

$$\overline{L_d} = a_1 + b_1 z \quad (z_1 < z < z_c)$$
$$\overline{L_d} = a_2 + b_2 z \quad (z_c < z < z_2), \tag{A.4}$$

where z_c is height of maximum canopy density, and a_1, b_1, a_2, b_2 are constants obtained from the solution of

$$\int_{z_1}^{z_2} \overline{L_d} dz = L_{t_c}.$$

Combination of (A.1) through (A.4) yields

$$\frac{\partial^2 y}{\partial z^2} = (A_i + B_i z) y, \tag{A.5}$$

where $y = u^2$, $A_i = \dfrac{2a_i C_d}{p_s \sigma}$, $B_i = \dfrac{2b_i C_d}{p_s \sigma}$, and $i = 1$ or 2 depending on $z \lessgtr z_c$.

Equation (A.5) may be solved to give an expression for the wind profile within the canopy that incorporates the modified Bessel function, $I_{1/3}$, and the modified Bessel function of the second kind (the MacDonald function), $K_{1/3}$

$$y = u^2 = \alpha_i Y_\alpha + \beta_i Y_\beta \tag{A.6}$$
$$Y_\alpha = \sqrt{\eta} I_{1/3}(\xi)$$
$$Y_\beta = \sqrt{\eta} K_{1/3}(\xi)$$
$$\eta = B_i^{-2/3}(A_i + B_i z)$$
$$\xi = \frac{2}{3}\eta^{3/2},$$

where α_i, β_i are constants determined from the solution of (A.6) with boundary conditions.

The gradient of the wind speed within the canopy air space is obtained from the derivative of (A.6):

$$\frac{dy}{dz} = \frac{d(u^2)}{dz} = \alpha_i \frac{dY_\alpha}{dz} + \beta_i \frac{dY_\beta}{dz}$$
$$\frac{dY_\alpha}{dz} = B_i^{1/3} \eta I_{-2/3}(\xi) = B_i^{1/3}\left[\eta I_{4/3} + \frac{I_{1/3}}{\sqrt{\eta}}\right]$$
$$\frac{dY_\beta}{dz} = B_i^{1/3}\left[-\eta K_{4/3} + \frac{K_{1/3}}{\sqrt{\eta}}\right] = B_i^{1/3} \eta K_{1/3}(\xi). \tag{A.7}$$

We have expressed the solution to (A.7) in positive indexes as these are required by the IMSL (1984) subroutines.

Equations (A.6) and (A.7) provide us with descriptions of the variation of u and K_m ($=\sigma u$) with height within the canopy. These are solved with boundary conditions imposed at the top and bottom of the canopy, see section c of this appendix. The modification of the wind profile description above the canopy is discussed in the next section.

b. Modification of the wind profile above the canopy

It is assumed that the log-linear wind profile holds good above a certain transition height, z_m. Experimentalists have noted that close to the canopy (i.e., below this height), the momentum transfer coefficient is augmented, presumably by the intense turbulence generated by roughness elements at the top of the canopy; see Raupach and Thom (1982), and Garratt

(1978). We assume that the height of the transition layer is a linear function of the roughness length, z_0.

$$z_m = z_2 + G_4 z_0, \tag{A.8}$$

where G_4 is a constant. (G_1, G_2 and G_3 are used to refer to related constants here and in Sellers et al. 1986).

We retain the assumption that the actual value of the momentum transfer coefficient, K_m, at z_2 is equal to a multiple of the estimate obtained from extrapolation of the log-linear profile as would be observed above z_m:

$$\begin{aligned} K_m &= G_1 K_m^*; \quad z = z_2 \\ &= G_1 k u_* (z_2 - d); \quad z = z_2, \end{aligned} \tag{A.9}$$

where G_1 is a constant; K_m^* is the value of K_m obtained from extrapolation of the log-linear wind profile ($m\ s^{-2}$), i.e. $ku_*(z - d)$; k is von Karman's constant (0.41); u_* is friction velocity ($m\ s^{-1}$); and d is zero plane displacement height (m).

We further assume that K_m varies linearly between z_2 and z_m, where it becomes equal to K_m^*. This yields

$$K_m = ku_*(z - d)\left[1 + (G_1 - 1)\left[\frac{z_m - z}{z_m - z_2}\right]\right] \qquad z_2 < z < z_m. \tag{A.10}$$

Now it is necessary to obtain values of the aerodynamic resistance of momentum transfer between z_2 and greater heights. These are obtained from the inverse integral of (A.9) or (A.10):

$$r_{a_m}|_{z_2}^{z} = \int_{z_2}^{z} \frac{1}{K_m}\, dz, \tag{A.11}$$

where $r_{a_m}|_{z_2}^{z}$ = aerodynamic resistance between z_2 and z, $s\ m^{-1}$.

When z is less than z_m, (A.10) can be inserted into (A.11) and integrated analytically. When z is greater than z_m, the inverse of (A.10) is integrated between z_2 and z_m and then added to the integral of the inverse of K_m^* from z_m to z.

c. *Solution of momentum transfer equations in the canopy*

The equation set governing momentum transfer within the canopy, (A.1) to (A.7), may be solved with suitable boundary conditions to yield profiles of u and K_m below z_2 and the value of d.

1) AT THE TOP OF THE CANOPY, z_2

Wind speed is taken as unity:

$$u, u^2, y = 1; \quad z = z_2. \tag{A.12}$$

Continuity of shear stress at z_2:

$$\begin{aligned} \tau|_{z \leqslant z_2} &= |\tau_{z \geqslant z_2} \\ \sigma u \frac{\partial u}{\partial z} &= \left[\frac{K_m}{G_1 k (z_2 - d)}\right]^2 \\ d &= z_2 - \frac{1}{G_1 k}\left(\frac{\sigma u}{\partial u / \partial z}\right)^{1/2}. \end{aligned} \tag{A.13}$$

2) AT THE CANOPY DENSITY INFLECTION POINT, z_c

Continuity of wind speed:

$$u^2|_{z_c \leqslant z} = u^2|_{z_c \geqslant z}. \tag{A.14}$$

Continuity of wind speed gradients:

$$\left.\frac{\partial (u^2)}{\partial z}\right|_{z_c \leqslant z} = \left.\frac{\partial (u^2)}{\partial z}\right|_{z_c \geqslant z}. \tag{A.15}$$

3) AT THE CANOPY BASE, z_1

Continuity of shear stress:

$$\frac{\sigma}{2}\frac{\partial (u^2)}{\partial z} = C_{D_{gs}} u^2, \tag{A.16}$$

where $C_{D_{gs}}$ is ground drag coefficient, equalling $[k/\ln(z_1/z_{gs})]^2$.

4) ZERO PLANE DISPLACEMENT HEIGHT, d

Thom (1971) defined the zero plane displacement height as equivalent to the moment height of momentum absorption by the surface. We may therefore write d as follows:

$$d = \frac{\int_{z_1}^{z_2} u^2 z\, dz}{\int_{z_1}^{z_2} u^2\, dz + \left.\frac{\tau}{\rho}\right|_{z_1} \frac{p_s}{L_d C_d}}. \tag{A.17}$$

If we substitute (A.4), (A.6) and (A.7) for u^2 and $\partial(u^2)/\partial z$ in the equation set (A.12) to (A.17), we have six equations in six unknowns; σ, d, a_1, b_1, z_2, and b_2. This set may be solved to yield the profiles of u and K_m and the value of d.

d. *Matching within canopy and above canopy transfer conditions*

The within and above canopy transfer conditions must be matched at z_2 to ensure continuity of wind speed and shear stress. Implicit in this calculation is the value of z_0, which may be determined from a consideration of the momentum balance at a height, z_x, above the canopy. This may be presented in terms of the definition of u_* as a function of the difference in wind speeds over a given height:

$$u_*^2 = \frac{(u_x - u_2)}{r_{a_m}|_{z_2}^{z_x}}, \tag{A.18}$$

where u_x is wind speed at z_x (m s^{-1}) and $r_{a_m}|_{z_2}^{z_x}$ is the aerodynamic resistance (s m^{-1}) for momentum between z_2 and z_x.

The aerodynamic resistance term in (A.18) is obtained from (A.11).

For the apparent value of z_0 at z_x, we may write

$$u_x = \frac{u_*}{k} \ln\left(\frac{z_x - d}{z_0}\right), \tag{A.19}$$

and for u_2, we may write

$$u_2 = \frac{G_1 k u_* (z_2 - d)}{\sigma}. \tag{A.20}$$

When we combine (A.19) and (A.20) with (A.18) we obtain an expression for z_0 in terms of z_x, G_1, d and z_m. Since z_m is a function of z_0 [see (A.8)], we must solve (A.18) with (A.8) iteratively.

This solution for z_0 gives rise to an interesting dependence of z_0 upon z_x. When $z_x > z_m$, z_0 is invariant with z_x, i.e., the log-linear profile holds good. When z_x is less than z_m, as is the case when an anemometer is sited within the transition layer above a canopy, z_0 appears to be dependent upon z_x.

Solution of the above equation set is fairly straightforward and is carried out in much the same way as was done for the original constant density canopy of Sellers et al. (1986). The only substantial changes are that the value of d in (A.16) has to be calculated numerically and that (A.8) and (A.20) have to be solved iteratively.

The other parameters associated with the aerodynamic transfer pathway are calculated much as before.

e. Calculation of aerodynamic resistances

Canopy bulk boundary layer resistance, $\overline{r_b}$, is defined as

$$\frac{1}{\overline{r_b}} = \int_{z_1}^{z_2} \frac{\overline{L_d}\sqrt{u}}{p_s C_s}\, ds, \tag{A.21}$$

where C_s is the transfer coefficient.

Here, $\overline{L_d}$ varies with height, see (A.4) and u is given by (A.6). (A.21) is then integrated numerically to give

$$\overline{r_b} = \frac{C_1}{\sqrt{u_2}}. \tag{A.22}$$

The ground to canopy air space resistance, r_d, is defined as before by

$$r_d = \int_{z_{gs}}^{h_a} \frac{1}{K_s}\, dz, \tag{A.23}$$

where h_a is center of action of $\overline{r_b}$ in the canopy (m), and K_s is heat/water vapor transfer coefficient (m s^{-2}), assumed to be equal to K_m. Equation (A.23) is integrated numerically using (A.16) below z_1 and (A.3) and (A.6) between z_1 and h_a to yield

$$r_d = \frac{C_2}{u_2}. \tag{A.24}$$

Canopy source height, h_a, is assumed to be equal to the center of action of $\overline{r_b}$ within the canopy as obtained from the solution of

$$\int_{z_1}^{h_a} \frac{L_d}{r_b} = \int_{h_a}^{z_2} \frac{L_d}{r_b}\, dz = \frac{1}{2\overline{r_b}}. \tag{A.25}$$

The aerodynamic resistance governing the transfer of heat and vapor between h_a and the reference height, z_r, is given by

$$r_a = \int_{h_a}^{z_r} \frac{1}{K_s}\, dz = \int_{h_a}^{z_2} \frac{1}{K_s}\, dz + \int_{z_2}^{z_m} \frac{1}{K_s}\, dz + \int_{z_m}^{z_r} \frac{1}{K_s}\, dz. \tag{A.26}$$

Equation (A.26) is calculated as the sum of the resistances acting within the separate regimes of the canopy air space $h_a < z < z_2$, the transition layer $z_2 < z < z_m$ and within the inertial sublayer $z_m < z$.

From the above, we see that we can obtain the surface parameters z_0 and d, and the resistance coefficients necessary for the calculation of $\overline{r_b}$, r_d and r_a, given values of the morphological parameters z_2, z_c, z_1, z_{gs}, $\overline{L_d}$, C_d and p_s, and the adjustment coefficients G_1 and G_4; see (A.8) and (A.9). Previously, G_1 and another related adjustment coefficient, G_2, were estimated from data. This time, we have decided to obtain the values of G_1 and G_4 that yield the best agreement of calculated values of z_0 and d with the results of Shaw and Pereira (1982). Figure A1 shows how z_0 and d vary with canopy drag coefficient as calculated from the model of Shaw and Pereira (1982). Points were taken off Fig. A1a corresponding to the numbers on the X-axis and were used as data against which the current model was forced to obtain best fit values of z_0 and d. An iterative minimization program ZXSSQ, published by IMSL (1984), was used to minimize the function $\sum_j F_1^2(z_0)_j + \sum_j F_2^2(d)_j$, where

$$F_{1(z_0)_j} = \left[\frac{z_{0_j}}{z_2}\right]_{\text{SP}} - \left[\frac{z_{0_j}}{z_2}\right]_{\text{SiB}} \tag{A.27}$$

$$F_{2(d)_j} = 0.1\left\{\left[\frac{d_j}{z_2}\right]_{\text{SP}} - \left[\frac{d_j}{z_2}\right]_{\text{SiB}}\right\} \quad j = 1, M, \tag{A.28}$$

where $F_{1(d)_j}$, $F_{2(z_0)_j}$ are the error for the jth estimate of d, z_0 provided by the SiB model; j is the index of z_0, d data pairs; M is the total number of z_0, d pairs used in minimization, which equals 28 (see Fig. A1); SP is subscript denoting Shaw and Pereira (1982) values; and SiB is subscript denoting SiB values.

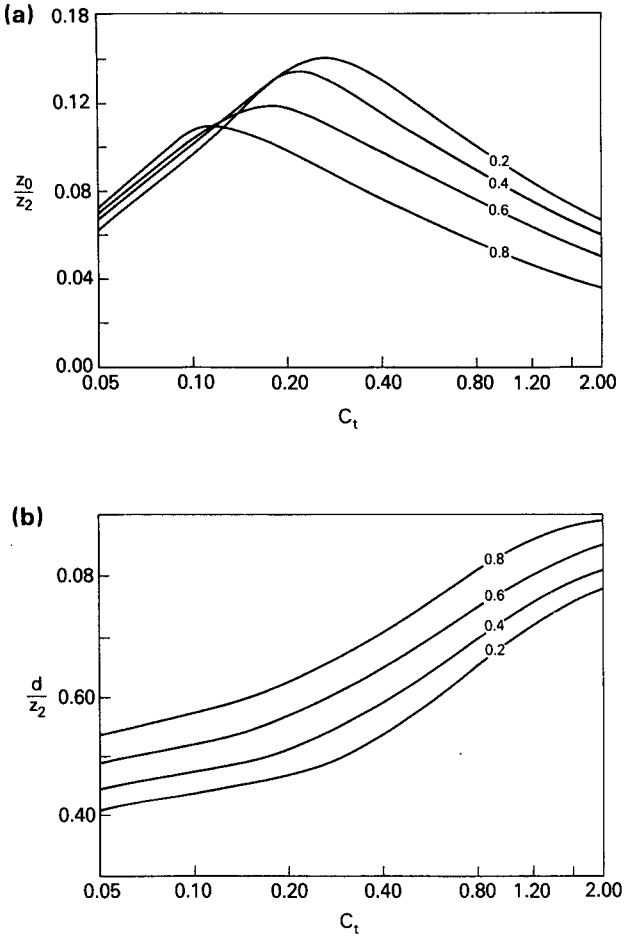

FIG. A1. Results of the Shaw and Pereira (1982) calculations. (a) Variation of the roughness length, z_0, with canopy drag coefficient, C_t, and height of maximum foliage density, z_c. (b) Variation of the zero plane displacement height, d, with canopy drag coefficient, C_t, and height of maximum foliage density, z_c. Canopy drag coefficient is given by $C_t = (C_d/p_s)\,L_t$. Height of maximum foliage density, z_c, divided by the canopy height, z_2, is marked on graph.

The zero plane displacement error, $F_{(d)}$, was weighted by 0.1 to give it an absolute value comparable to $F_{(z_0)}$.

This procedure yielded the following parameter values;

$$G_1 = 1.449$$

$$G_4 = 11.785. \qquad \text{(A.29)}$$

The results shown in (A.29) are acceptable from a physical viewpoint. The data of Garratt (1978) suggests that G_1 lies in the range of 1.5 to 2. The transition layer is estimated by SiB to extend roughly 12 times ($G_4 \approx 12.0$) the height of the roughness length above the canopy top; that is, to about 2–2.5 times the height of the vegetation.

Figure A2 shows the variation of z_0 and d as calculated by the SiB model using (A.29). This may be compared to Fig. A1.

Figure A3 shows how the updated model performs relative to the old constant density canopy formulation. The wind profile compares better with observations in the upper half of the canopy, d is raised and z_0 is lowered, mainly because z_c is closer to z_2 than to z_1 (z_c was estimated by the second author to be at roughly 80 percent of the height difference between z_1 and z_2). This has the effect of reducing the calculated u_*/u_r values to give closer agreement with observations; see Fig. 5b and 5d. The wind profiles calculated with the new model provide a poor match to observations in the lower part of the canopy, the so-called trunk space, while matching observations fairly well near the canopy

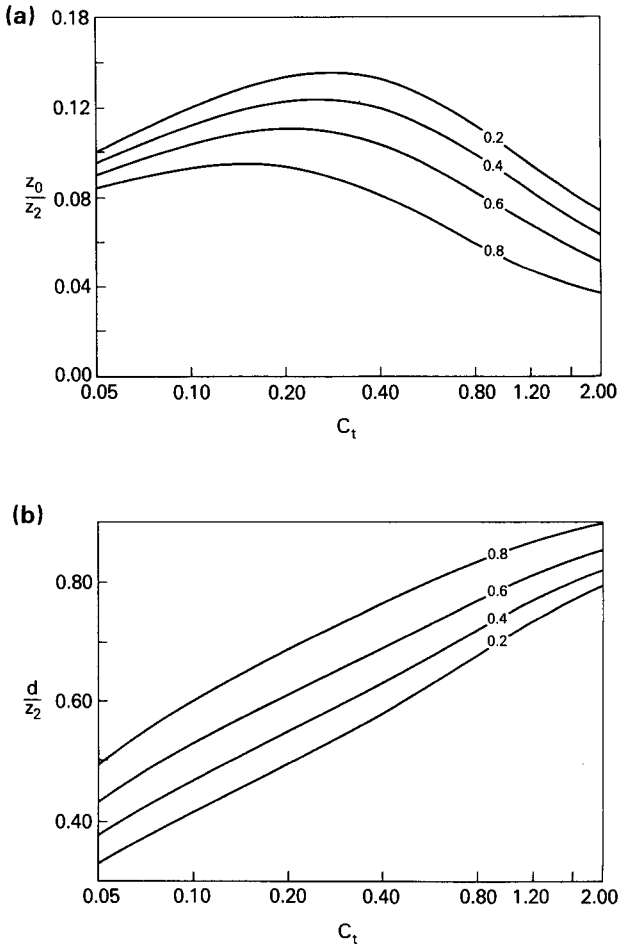

FIG. A2. Results of SiB aerodynamic (preprocessor) model with parameters forced to match the results of Shaw and Pereira (1982). (a) Variation of the roughness length, z_0, with canopy drag coefficient, C_t, and height of maximum foliage density, z_c. (b) Variation of the zero plane displacement height, d, with canopy drag coefficient, C_t, and height of maximum foliage density, z_c. Canopy drag coefficient is given by $C_t = (C_d/p_s)\,L_t$. Height of maximum foliage density, z_c, divided by canopy height, z_2, is marked on graph.

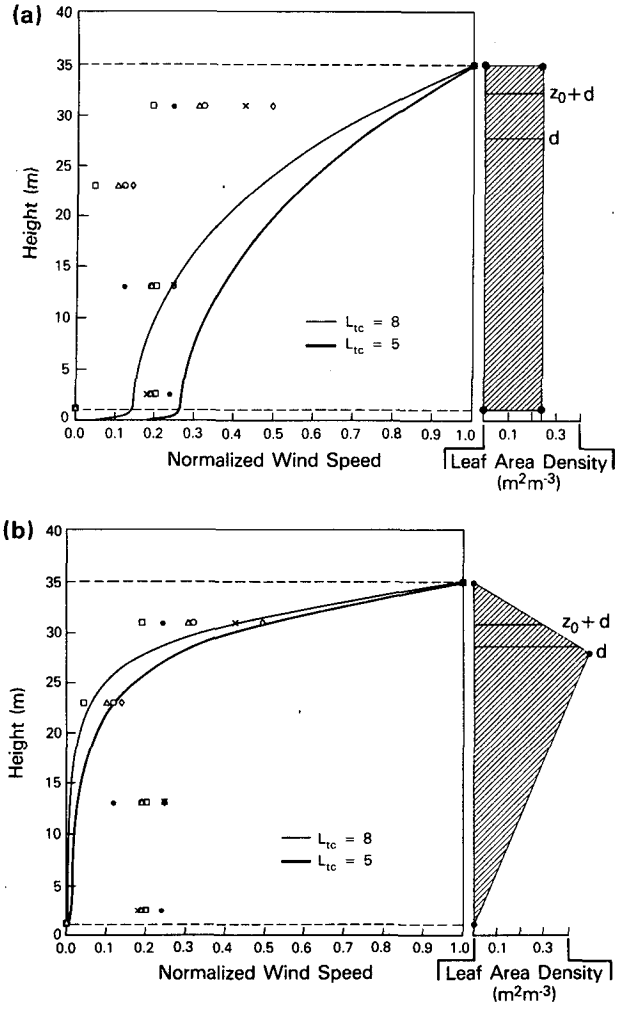

FIG. A3. Profiles of leaf area density, L_d, and normalized wind speed as calculated by (a) the old constant density foliage distribution aerodynamic model and (b) the new triangular foliage distribution aerodynamic model. The heights of z_0 and d are also marked. Note that two values for the total leaf area index, L_t, are used, 8.00 and 5.01. Normalized wind speed observations, (u/u_2), from Roberts et al. (1989) are shown for comparison.

top where most of the momentum and heat fluxes are exchanged. It is doubtful whether a first-order closure model can ever represent transfer processes below the canopy in a realistic fashion (see Shaw and Pereira 1982).

APPENDIX B

Physiological Parameters as Obtained from a Review of the Ecological Literature and Data from Pearcy (1987) and Roberts et al. (1989)

A number of studies reported in the ecological literature were reviewed in order to obtain an estimated mean physiological parameter set for the tropical forest. The parameters of greatest interest are those governing the stomatal response to changing photosynthetically active radiation (PAR) flux density (a, b, c) and the parameter that determines the rate of stomatal resistance increase for increasing values of the ambient vapor pressure deficit, h_5.

a. Literature review parameter set

Usable curves of leaf stomatal resistance versus PAR were collated for eight tropical forest vegetation types/states, listed in Table B1. These curves vary considerably both in typical magnitude and response to changing PAR flux density. In order to provide some estimate of average behavior, three PAR or solar radiation regimes were defined (Table B2) PAR flux is simply estimated as half the solar flux, following Goudriaan (1977). The ratios of r_s values in each regime were taken in order to specify the *relative* response of r_s to PAR flux density. These results are also listed in Table B.1. In each case, an attempt was made to use r_s values obtained when the vapor pressure deficit, δe, was 6 mb or less, or the relative humidity was 80 percent or more. The average values given in Table B.3 were used to define the shape of the average PAR response curve. It is then necessary to specify an absolute value for r_s, preferably in the light-saturated (γ) regime. A median value was taken from Fig. 3 from Chiarello (1984), which shows the diurnal range of stomatal conductance for a number of tropical species, assuming this median value corresponds to a PAR flux density of 200 W m^{-2}. The median value obtained was 0.55 mol m^{-2} s^{-1} or 1.4 cm s^{-1}. Assuming a value of h_5 = 0.038 (calculated for these data using the method specified below) and a value of δe of 6 mb, we obtain a value of 1.81 cm s^{-1} for the unstressed stomatal conductance. This was combined with a calculation involving the ratios shown in Table B1 to calculate values of a, b, c, as reproduced in Table 3, column I. The resistance/conductance values calculated from these parameters for typical daytime conditions correspond to estimates supplied by a number of researchers via personal communication, i.e., leaf conductances of 1.5–2.5 cm s^{-1}.

Equation (13) in the text is used to relate the minimum value of the stomatal resistance, determined from the light dependent part of Eq. (10) to its actual value in the presence of a vapor pressure deficit. We made use of the data reproduced in Fig. 4 of Grace et al. (1982) which summarized observations made on tropical timber trees. The data of Chiarello (1984) and Mooney et al. (1984) were also studied. Fitting of Eq. (13) to these data and averaging the result yielded an estimate of h_5 = 0.022 mb^{-1}. (Note: This is different from the value of 0.038 mb^{-1} used in the previous section which is relevant only to the Chiarello 1984 data.)

TABLE B1. Tropical species for which stomatal resistance characteristics have been published. Ratio I is the ratio of the stomatal resistance measured at PAR = 100 W m^{-2} to that at PAR = 0.0 W m^{-2}. Ratio II is the ratio of stomatal resistance values measured at PAR = 100 W m^{-2} to that measured at PAR = 500 W m^{-2}. The vapor pressure deficit in the first four and the last two cases was about 6 mb. These data were combined to produce the literature review parameter set discussed in the text. Note that the Tectona grandis is not native to Nigeria; the measurements were conducted in a plantation.

Vegetation type	Location	Ratio I	Ratio II	Source
Tectona grandis (wet season)	Nigeria	0.22	2.07	Grace et al. (1982)
Tectona grandis (dry season)	Nigeria	0.19	1.38	Whitehead et al. (1981)
Gmelina arborea (wet season)	Nigeria	0.67	3.41	Grace et al. (1982)
Gmelina arborea (dry season)	Nigeria	0.21	3.21	Whitehead et al. (1981)
Piper auritum	Mexico	0.57	2.26	Chiariello (1984)
Piper hispidium	Mexico	0.24	1.18	Mooney et al. (1984)
Euphorbia forbesii	Hawaii	0.29	1.08	Pearcy and Calkin (1983)
Claoxylon sandwicense	Hawaii	0.21	1.13	Pearcy and Calkin (1983)
Mean		0.32	1.97	

TABLE B2.

Regime	PAR flux (W m^{-2})	Solar flux (W m^{-2})
α	0	0
β	100	200
γ	500	1000

b. *Pearcy parameter set*

Pearcy (1987) reported leaf stomatal resistance and photosynthetic rates as functions of PAR, leaf water potential, air temperature and vapor pressure deficit for two tree species in an Australian tropical forest. Data from the paper of Pearcy (1987) were selected on the basis of low ambient vapor pressure deficits in order to obtain a description of the unstressed leaf stomatal response to PAR. These data, for two species, are shown in Fig. B1 together with the best fit of (10) in text. Other data in Pearcy (1987) were analyzed to give estimates of $h_5 = 0.0270$ and 0.0182 for Toona australis and Argyrodendron peralatum, respectively, and hence a mean value of $h_5 = 0.0226$. The Pearcy parameter set may be found in Table 3, column II.

c. *Roberts et al. parameter set*

Roberts et al. (1989) visited the site three times during the course of the experiment: September–October 1983, July–August 1984, and March–April 1985. During these visits, leaf water potential measurements were made throughout the depth of the canopy and averaged to provide mean canopy leaf water potential estimates for two tree species, Piptadenia suavolens and Bocoa viridiflora (see text). Additionally, a large number of stomatal conductance, $g_s (g_s = 1/r_s)$, measurements were made on four tree species, distributed throughout the depth of the canopy. The leaf water potential measurements were used for the optimization procedure described in the text and so are not discussed here.

Roberts et al. (1989) analyzed their stomatal con-

TABLE B3. Results of reanalysis of the in situ leaf stomatal resistance observations of Roberts et al. (1989) and results of SiB calculations for the same periods. The figures in the tables refer to the derivative of the product of the stomatal stress factors governed by leaf water potential and vapor pressure deficit with respect to increasing vapor pressure deficit. More succinctly, the values shown are b where

$$b = -\frac{\partial[f(\psi_l)f(\delta e)]}{\partial(\delta e)}. \quad \text{(B.1)}$$

Values of b are determined from least-squares regression on stomatal resistance data from Roberts et al. (1989) data (b_R) and the simulation results produced by SiB (b_s). For the observations, δe was estimated within the canopy air space; for the SiB results, an equivalent figure is provided by $\delta e = e^*(T_a) - e_a$ (see text).

Above canopy shortwave radiation (W m^{-2})	Piptadenia suavolens	Licania micranthia	Bocoa viridiflora	Naucleopsis glabra	Mean of all species	Calculated from SiB
701–800	0.043	—	—	—	0.043	0.032
601–700	0.032	0.036	0.038	0.049	0.039	0.032
501–600	0.036	0.044	0.047	0.055	0.046	0.033
401–500	0.035	0.042	0.037	0.048	0.041	0.033
<400	0.028	0.050	0.039	0.048	0.041	0.031
Mean within species	0.035	0.043	0.040	0.050	0.042	0.032

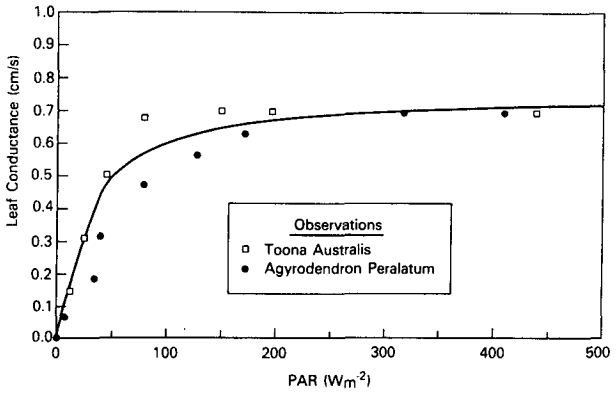

FIG. B1. Maximum stomatal conductance data for two Australian tropical forest species plotted against PAR flux density normal to the leaf surface, data from Pearcy (1987). The line shows best fit of Eq. (10) in text.

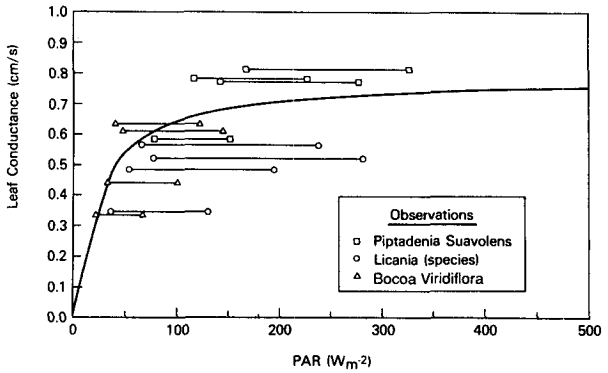

FIG. B2. Maximum stomatal conductance data for four Amazonian tropical forest species plotted against PAR flux density normal to the leaf surface, data from Roberts et al. (1989). The horizontal bars show the range of PAR flux densities calculated for the top and midpoint of each species canopy as described in text. The line shows best fit of Eq. (10) in text.

ductance data by dividing them into strata on the bases of:

(i) Above canopy incident shortwave flux. (Five categories were used: <400, 401–500, 501–600, 601–700 and 701–800 W m^{-2}.)

(ii) Species: Four species were sampled with foliage midheights ranging from 33.4 m (canopy top) to 19.6 m (below about 60 percent of the foliage).

(iii) Specific humidity deficit (δq): values of within-canopy δq ranging from 2 to 14 g kg^{-1} were observed.

Roberts et al. (1989) performed regression analysis (g_s against δq) on the data within radiation and species strata. In the current analysis, we have assumed the intercept of these regressions, A_R, to be the maximum conductance for the species multiplied by $f(T)$ (assumed to be about unity) and the slope, B_R, to be due to the combined effect of $f(\delta e)$ and $f(\psi_l)$; see Eq. (10) in text for explanation of symbols. The slopes published by Roberts et al. (1989) were transformed to yield slopes of the relative decrease in g_s as a function of δe by

$$b_R = \frac{-B_R}{A_R}\left(p\frac{217}{T_r}\right) = \frac{-\partial(f(\delta e)f(\psi_l))}{\partial(\delta e)}, \quad \text{(B.1)}$$

where A_R is intercept of regression of g_s against δq (cm s^{-1}), B_R is slope of regression of g_s against δq (cm s^{-1} g^{-1} kg), p is atmospheric pressure (mb), and T_r is reference temperature (K). These b_R values are reproduced for the four species in question in Table B3 where they are compared to equivalent values calculated by SiB.

The contemporaneous radiation data available to Roberts et al. (1989) consisted only of shortwave fluxes above the canopy. Here we have assumed the triangular foliage density distribution as described in appendix A, a planophile ($\chi_L = 0.1$) leaf angle distribution, and a solar zenith angle of 20°, and have used the species foliage top and midpoint height data of Roberts et al. (1989) to estimate PAR flux densities normal to the leaf surfaces at the tops and midpoints of each species' canopy. The A_R (maximum g_s) values were then plotted against these calculated PAR flux densities (see Fig. B2), it being assumed that the data of Roberts et al. (1989) were collected from the upper half of each tree sampled. A best fit of Eq. (10) was then made to these data and the resultant coefficients are shown in Table 3, column IV.

REFERENCES

Baldocchi, D. D., B. A. Hutchinson, D. R. Matt and R. T. McMillen, 1985: Canopy radiative transfer models for spherical and known leaf inclination angle distributions: a test in an oak-hickory forest. *J. Appl. Ecol.*, **22**, 539–555.

Charney, J. G., W. J. Quirk, S. H. Chow and J. Kornfield, 1977: A comparative study of the effects of albedo change on drought in semi-arid regions. *J. Atmos. Sci.*, **34**, 1366–1385.

Chiariello, N., 1984: Leaf energy balance in the wet lowland tropics. *Physiological ecology of plants of the wet tropics*, E. Medina, H. A. Mooney and C. Vazquez-Yanes, Eds., W. Junk, 254 pp.

Choudhury, B. J., 1983: Simulating the effects of weather variables and soil water potential on a corn canopy temperature. *Agric. Met.*, **29**, 169–182.

Clapp, R. B., and G. M. Hornberger, 1978: Empirical equations for some soil hydraulic properties. *Water Resour. Res.*, **14.4**, 601–604.

Davies, W. J., J. Metcalfe, T. A. Lodge and A. R. Costa, 1986: Plant growth substances and the regulation of growth under drought. *Aust. J. Plant Physiol.*, **13**(1), 105–125.

Deardorff, J. W., 1978: Efficient prediction of ground surface temperature and moisture, with inclusion of a layer of vegetation. *J. Geophys. Res.*, **83**, 1889–1903.

Dickinson, R. E., 1983: Land surface processes and climate-surface albedos and energy balance. *Advances in Geophysics*, Vol. 25, Academic Press, 305–353.

——, 1984: Modelling evapotranspiration for three-dimensional global climate models. *Climate Processes and Climate Sensitivity, Geophysical Monogr.*, N. 29, J. E. Hanson and T. Takahashi, Eds., American Geophysical Union, 58–72.

Dorman, J. L., and P. J. Sellers, 1989: A global climatology of surface parameters for atmospheric general circulation models as represented by the Simple Biosphere model (SiB). *J. Climate*, in press.

Federer, C. A., 1979: A soil-plant-atmosphere model for transpiration

and availability of soil water. *Water Resour. Res.*, **15.3**, 555–562.

Garratt, J. R., 1978: Flux profile relations above tall vegetation. *Quart. J. Roy. Meteor. Soc.*, **104**, 199–211.

Goudriaan, J., 1977: *Crop Micrometeorology: A Simulation Study.* Wageningen Center for Agricultural Publishing and Documentation, 249 pp.

Grace, J., D. U. Okali and F. E. Fasehun, 1982: Stomatal conductance of two tropical trees during the wet season in Nigeria. *J. Appl. Ecol.*, **19**, 659–670.

Hancock, N. H., and J. M. Crowther, 1979: A technique for the direct measurement of water storage on a forest canopy. *J. Hydrol.*, **41**, 105–122.

——, P. J. Sellers and J. M. Crowther, 1983: Evaporation from a partially wet forest canopy. *Ann. Geophys.*, **I**(2), 139–146.

IMSL (International Mathematical and Statistical Library), 1984: Chapter Z. IMSL, ZXSSQ-1 to ZXSSQ-7.

Jarvis, P. G., 1976: The interpretation of the variations in leaf water potential and stomatal conductance found in canopies in the field. *Philos. Trans. Roy. Soc. London, Ser. B*, **273**, 593–610.

Jordan, C. F., and G. Escalante, 1980: Root productivity in an Amazonian rain forest. *Ecology*, **61**(1), 14–18.

Larcher, W., 1969: The effect of environmental and physiological variables on the carbon dioxide gas exchange of trees. *Photosynthetica*, **3**(2), 167–198.

Lloyd, C. R., and A. de O. Marques, 1988: Spatial variability in rainfall interception measurements in Amazonian rain forest. *Agric. For. Met.*, **42**, 63–73.

——, W. J. Shuttleworth, M. Turner and J. H. C. Gash, 1984: A microprocessor system for eddy-correlation. *Agric. For. Met.*, **33**, 67–80.

Meador, W. E., and W. R. Weaver, 1980: Two-stream approximations to radiative transfer in planetary atmospheres: A unified description of existing methods and a new improvement. *J. Atmos. Sci.*, **37**, 630—643.

Medina, E., and H. Klinge, 1983: Productivity of tropical forests and tropical woodlands. *Physiological Plant Ecology IV*, O. L. Lange, P. S. Nobel, C. B. Osmond and H. Ziegler, Eds., Springer-Verlag, 644 pp.

Milly, P. C., and P. S. Eagleson, 1982: Parameterization of moisture and heat fluxes across the land surface for use in atmospheric General Circulation Models. Rep. 279, Dept. of Engineering, Massachusetts Institute of Technology, 159 pp.

Monteith, J. L., 1973: *Principles of Environmental Physics.* Edward Arnold Ltd., 242 pp.

Mooney, H. A., C. Field and C. Vazquez-Yanes, 1984: Photosynthetic characteristics of wet tropical forest plants. *Physiological Ecology of Plants of the Wet Tropics*, E. Medina, H. A. Mooney and C. Vazquez-Yanes, Eds., W. Junk, 254 pp.

Moore, C. J., 1986: Frequency response corrections for eddy correlation systems. *Bound.-Layer Meteor.*, **37**, 17–35.

Mori, S. A., and B. M. Boom, 1987: Chapter II: The Forest. *The Lecythidaceae of a lowland neotropical forest: La Funee Mountain, French Guiana.* S. A. Mori and collaborators, Mem. New York. Bot. Gard., 9–29, 190 pp.

Pearcy, R. W., 1987: Photosynthetic gas exchange responses of Australian tropical forest trees in canopy, gap and understory microenvironments. *Functional Ecology*, **1**, 169–178.

——, and H. Calkin, 1983: Carbon dioxide exchange of C_3 and C_4 tree species in the understory of a Hawaiian forest. *Oecologia*, **S8**, 26–32.

Pinker, R. T., O. E. Thompson and T. F. Eck, 1980a: The energy balance of a tropical evergreen forest. *J. Appl. Meteor.*, **19**(12), 1341–1350.

——, —— and ——, 1980b: The albedo of a tropical evergreen forest. *Quart. J. Roy. Met. Soc.*, **106**, 551–558.

Pires, J. M., 1978: The forest ecosystems of the Brasilian Amazon: Description, functioning and research needs. *Tropical Forest Ecosystems*, rep. by UNESCO, UNEP and FAO, UNESCO, 607–627.

Ratisbona, L. R., 1976: The climate of Brazil. *World Survey of Climatology*, Vol. 12, W. Schwerdtferger, Ed., Elsevier, 219–269.

Raunkiaer, C., 1934: *The Life-Forms of Plants and Statistical Plant Geography.* Clarendon Press.

Raupach, M. R., and A. S. Thom, 1981: Turbulence in and above plant canopies. *Annual Review of Fluid Mechanics*, Vol. 13, 97–129.

Roberts, J., O. M. R. Cabral and L. F. de Aguiar, 1989: Stomatal and boundary-layer conductances measured in an Amazonian Terra Firme Rain Forest. *J. Appl. Ecol.* (in press).

Ross, J., 1975: Radiative transfer in plant communities. *Vegetation and the Atmosphere*, J. L. Monteith, Ed., Academic Press, 13–52.

Rutter, A. J., K. A. Kershaw, P. C. Robins and A. J. Morton, 1971: A predictive model of rainfall interception in forests. Part I: derivation of the model from observations in a plantation of Corsican pine. *Agric. Meteor.*, **9**, 367–384.

Schulze, E. D., 1982: Plant life forms and their carbon, water and nutrient relations. *Physiological Plant Ecology II*, O. L. Lange, P. S. Nobel, C. B. Osmond and H. Ziegler, Eds., Springer-Verlag, 747 pp.

Sellers, P. J., 1985: Canopy reflectance, photosynthesis and transpiration. *Int. J. Rem. Sens.*, **6**(8), 1335–1372.

——, and J. L. Dorman, 1987: Testing the Simple Biosphere model (SiB) using point micrometeorological and biophysical data. *J. Clim. Appl. Meteor.*, **26**(5), 622–651.

——, Y. Mintz, Y. C. Sud and A. Dalcher, 1986: A Simple Biosphere model (SiB) for use within General Circulation Models. *J. Atmos. Sci.*, **43**(6), 505–531.

Shaw, R. H., and A. R. Pereira, 1982: Aerodynamic roughness of a plant canopy: A numerical experiment. *Agric. Meteor.*, **26**, 51–65.

Shu Fen Sun, 1982: Moisture and heat transport in a soil layer forced by atmospheric conditions. M. S. Thesis, Dept. of Civil Engineering, University of Connecticut, 72 pp.

Shukla, J., and Y. Mintz, 1982: Influence of land-surface evapotranspiration on the earth's climate. *Science*, **215**, 1498–1501.

Shuttleworth, J. W., 1988: Evaporation from Amazonian rain forest. *Phil. Trans. Roy. Soc. London, Ser. B*, 233–346.

——, and I. R. Calder, 1979: Has the Priestley–Taylor equation any relevance to forest evaporation? *J. Appl. Meteor.*, **18**, 634–638.

——, and J. S. Wallace, 1985: Evaporation from sparse crops—an energy combination theory. *Quart. J. Roy. Meteor. Soc.*, **111**, 839–855.

——, J. H. C. Gash, C. R. Lloyd, C. J. Moore, J. Roberts, A. D. O. Marques Filho, G. Fisch, V. De Paula Silva Filho, M. De Nazare Goes Ribeiro, L. C. B. Molion, L. D. De Abreusa, J. Carlos, A. Nobre, O. M. R. Cabral, S. R. Patel and J. Carvalho De Moraes, 1984a: Eddy correlation of energy partition for Amazonian forest. *Quart. J. Roy. Meteor. Soc.*, **110**, 1143–1162.

—— et al., 1984b (authors same as above): Observations of radiation exchange above and below Amazonian forest. *Quart. J. Roy. Meteor. Soc.*, **110**, 1163–1169.

Sud, Y. C., J. Shukla and Y. Mintz, 1985: Influence of land-surface roughness on atmospheric circulation and rainfall: A sensitivity experiment with a GCM. NASA Tech. Memo. 86219.

Thom, A. S., 1971: Momentum absorption by vegetation. *Quart. J. Roy. Meteor. Soc.*, **97**, 414–428.

van der Honert, T. H., 1948: Water transport as a catenary process. *Discuss. Faraday Soc.*, **3**, 146–153.

Verma, S. B., D. D. Baldocchi, D. E. Anderson, D. R. Matt and R. J. Clement, 1986: Eddy fluxes of CO_2, water vapor, and sensible heat over a deciduous forest. *Bound.-Layer Met.*, **36**, 71–91.

Walker, J. M., and P. R. Rowntree, 1977: The effect of soil moisture on circulation and rainfall in a tropical model. *Quart. J. Roy. Meteor. Soc.*, **103**, 29–46.

Whitehead, D., D. U. Okali and F. E. Fasehun, 1981: Stomatal response to environmental variables in two tropical forest species during the dry season in Nigeria. *J. Appl. Ecol.*, **18**, 571–587.

Willmott, C. J., and K. Klink, 1986: A representation of the terrestrial biosphere for use in global climate studies. *ISLSCP: Proc. of an international conference held in Rome, Italy, 2–6 December 1985*, Rome, Italy, European Space Agency, 109–112.